Luminous type II Supernovae [*]

C. Inserra[1,2,3][**], A. Pastorello[4], M. Turatto[4], M. L. Pumo[4,5,6], S. Benetti[4], E. Cappellaro[4], M. T. Botticella[7], F. Bufano[8], N. Elias-Rosa[9], A. Harutyunyan[10], S. Taubenberger[11], S. Valenti[4], and L. Zampieri[4]

[1] Astrophysics Research Centre, School of Mathematics and Physics, Queen's University Belfast, Belfast BT7 1NN, United Kingdom
[2] Dipartimento di Fisica ed Astronomia, Università di Catania, Sezione Astrofisica, Via S.Sofia 78, 95123, Catania, Italy
[3] INAF - Osservatorio Astrofisico di Catania, Via S.Sofia 78, 95123, Catania, Italy
[4] INAF - Osservatorio Astronomico di Padova, Vicolo dell'Osservatorio 5, 35122, Padova, Italy
[5] Bonino-Pulejo Foundation, Via Uberto Bonino 15/C, I-98124 Messina, Italy
[6] Università di Padova, Dipartimento di Fisica ed Astronomia G. Galilei, Vicolo dellOsservatorio, 3, 35122 Padova
[7] INAF - Osservatorio astronomico di Capodimonte, Salita Moiariello 16, I- 80131 Napoli, Italy
[8] Departamento de Ciencias Fisicas, Universidad Andres Bello, Avda. Republica 252, Santiago, Chile
[9] Institut de Cincies de l'Espai (IEEC-CSIC), Campus UAB, 08193 Bellaterra, Spain
[10] Fundación Galileo Galilei-INAF, Telescopio Nazionale Galileo, Rambla José Ana Fernández Pérez 7, 38712 Breña Baja, TF - Spain
[11] Max-Planck-Institut für Astrophysik, Karl-Schwarzschild-Str. 1, 85741 Garching, Germany

ABSTRACT

Context. In this paper we present spectroscopic and photometric observation of five type II supernovae (SNe), namely SNe 2009dd, 2007pk, 2010aj, 1995ad, and 1996W. Together with other few SNe they form a group of luminous type II events.
Aims. We investigate the similarities and the differences among these five SNe, that represent the bulk of the luminous type II so far. We also attempt to characterise this subgroup of core-collapse SNe by analysing their spectral evolution, in order to find evidences of interaction that are common to them.
Methods. We collect data ranging from the ultraviolet (UV) to the near-infrared (NIR) with several telescopes in order to construct well-sampled light curves and spectral evolutions from the photospheric to the nebular phase. Both photometric and spectroscopic evolution indicate significant differences among the objects and between them and other luminous type II SNe. Modelling the data of SNe 2009dd, 2010aj and 1995ad allows us to constrain the explosion parameters and the properties of the progenitor star, and compare the inferred estimates with those available for the similar SNe 2007od and 2009bw.
Results. The light curves have luminous peak magnitudes $-18.70 < M_B < -17.18$ and a wide range of ^{56}Ni masses $7 \times 10^{-3} M_\odot < M_\odot(^{56}\text{Ni}) < 1.4 \times 10^{-1} M_\odot$. Only SN 2010aj does not follow the decay of ^{56}Co. Clues of interaction, such as the presence of high velocity (HV) features of the Balmer lines are visible in the photospheric spectra of SNe 2009dd, 1995ad and 1996W. Instead for SN 2007pk we observe a spectral transition from a type IIn to a standard type II. Modelling the observations with a radiation hydrodynamics code, we infer for SNe 2009dd, 2010aj and 1995ad a kinetic plus thermal energy of about 0.2–0.5 foe, an initial radius of 2–5×10^{13} cm and an ejected mass of ~ 5.0–9.5 $M_\odot$. The results suggest a super-asymptotic giant branch (SAGB) progenitor or a RSG exploded as a weak Fe CC-SN for these SNe, similarly to the other luminous type II SNe 2007od and 2009bw. The SNe analysed share only the high luminosity and the short plateau duration suggesting a sample far from homogeneity, but consistent with the bright branch of type II SNe. Such events might represent the link in the distribution of physical properties between standard type II and strong interacting type IIn SNe.

Key words. supernovae: general - supernovae: individual: SN 2009dd - supernovae: individual: SN 2007pk - supernovae: individual: SN 2010aj - supernovae: individual: SN 1995ad - supernovae: individual: SN 1996W

1. Introduction

It is widely accepted that type II Supernovae (SNe) constitute a very heterogeneous class. They stem from the collapse of the degenerate core of a sufficiently massive star (ZAMS mass $\gtrsim 8$ $M_\odot$, e.g. Smartt 2009; Pumo et al. 2009, and reference therein), in most cases a red supergiant (RSG). H rich progenitors are thought to produce type II "plateau" (IIP) SNe, which show a nearly constant luminosity (plateau phase) for a period of 2-3 months, during which the H envelope recombines, releasing the internal energy. The length of the plateau primarily depends of the mass of the H envelope. Instead, if the H envelope mass is very low, the light curve shows a linear, uninterrupted decline after maximum. These SNe are historically classified as type II "linear" (SNe IIL, Barbon et al. 1979). Intermediate cases have been found with light curves showing short or even only hints of a Plateau, e.g. SNe 1992H (Clocchiatti et al. 1996).

A common feature of the two mentioned sub-types is the late-time linear tail in the light curve produced by the energy release of the radioactive decay of ^{56}Co to ^{56}Fe with the characteristic slope of 0.98 mag/100d if complete γ-ray and e^+ trapping occurs. In some cases the observed decline rate is significantly modified by dust formation within the ejecta, which absorbs light at optical wavelengths and re-emits photons in the near infrared (NIR), or by the interaction of the fast ejecta with a slow circumstellar medium (CSM), which converts kinetic energy into radiation.

The very early-time spectra of most SNe IIP and IIL approximate a Planck function from UV through IR wavelengths. The spectra are dominated by P-Cygni profile of Balmer series lines with a strong Hα emission, while metal lines arise during the plateau. The late-time spectra of SNe IIP and IIL are dominated by relatively narrow emission lines of H and forbidden transitions of Ca II, O I, Fe II etc. (e.g. Turatto, Benetti, and Cappellaro 2003) and are called nebular.

A different subclass is that of SNe II with narrow emission lines already present at early phase (SNe IIn, Schlegel 1990). The spectra of these objects are dominated by strong H Balmer emission lines without the characteristic broad blue-shifted absorptions and have a slow time evolution due to the interaction between the ejecta and the CSM. The interaction of the fast ejecta with a slowly expanding, dense CSM generates a forward shock in the CSM and a reverse shock in the ejecta. The shocked material emits energetic radiation whose spectrum depends on the density of both the CSM and the ejecta, and on the properties of the shock (Chevalier & Fransson 1994). Sometimes the pressure and temperature behind the shock are sufficiently high that the post-shock ejecta and CSM becomes powerful X-rays emitters. At the same time synchrotron radiation is generated by electrons accelerated up to relativistic energies at the shock front. Thus the great diversity of observed SNe IIn provide clues to the different history of the mass-loss in the late evolution of their progenitors. Typical mass loss rates are of the order of 10^{-6}–10^{-5} $M_\odot yr^{-1}$, but this value may change significantly and can exceed 10^{-4} $M_\odot yr^{-1}$ (Chugai 1994) as shown by Zampieri et al. (2005) for SN 1995N.

Sometimes normal SNe II, most often of the "linear" sub-type e.g. SNe 1979C Milisavljevic et al. (2009, and references therein), 1980K Milisavljevic et al. (2012, and references therein), 1986E Cappellaro et al. (1995), after a normal evolution from the photospheric to nebular phase, show the onset of ejecta-CSM interaction. It is interpreted as evidence that the ejecta after a phase of free expansion reaches dense material ejected by the progenitor during episodes of strong mass loss ceased a few $10^2 - 10^3$ yr before the explosion. Recently a few SNe with overall normal spectral features have shown weak but unequivocal evidence of ejecta-CSM interaction from early times, reviving the interest for the studies of interacting SNe. Among them we recall the type IIP SNe 1999em and 2004dj (Chugai et al. 2007) or other "atypical" type II SNe as SN 2007od (Inserra et al. 2011) and SN 2009bw (Inserra et al. 2012a), the last two objects belonging to the bright end of the type IIP SN luminosity distribution.

In this paper we present the spectroscopic and photometric observations of five bright objects, the type II SNe 2009dd, 2007pk and 2010aj, plus unpublished archive data of two objects, SN 1995ad and SN 1996W. Together with other four SNe (SNe 1992H, 2004et, 2007od and 2009bw) these make up almost all that is available for this bright end of the type II SNe. The common feature of these objects are the high peak luminosity and the short plateau duration. Some of the SNe here pre-
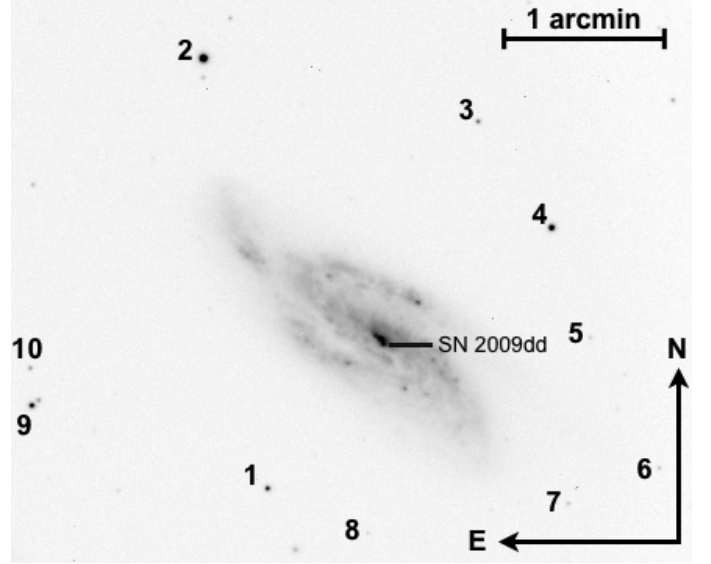

Fig. 1. R band image of SN 2009dd in NGC 4088 obtained with CAHA+CAFOS on November 19th, 2009. The sequence of stars used to calibrate the optical and NIR magnitudes is indicated.

sented should be added to the number of overall normal core-collapse SNe with signature of early but not dominant ejecta-CSM interaction. The plan of the paper is the following: in Sect. 2 we introduce the SNe and their host galaxy properties, estimating distances and reddening values. Photometric data, light and colour curves as well as the estimates of ^{56}Ni masses are presented in Sect. 3; in Sect. 4 we describe and analyse the spectra; a discussion is presented in Sect. 5, while a short summary follows in Sect. 6.

2. SNe and their host galaxies

In this Section the selected SNe and their host galaxies are presented individually. We adopt a cosmology with $H_0 = 73$ km s^{-1}Mpc^{-1}, $\Omega_m = 0.27$ and $\Omega_\lambda = 0.73$ throughout the paper.

1. SN 2009dd (Fig. 1) was discovered in the SABbc galaxy NGC 4088 by Cortini & Dimai (2009) on 2009 April 13.97. Elias-Rosa et al. (2009) classified the object as a young type II SN with strong NaID interstellar features indicating significant absorption inside the parent galaxy.
   Prompt observations with Swift+XRT revealed an X-ray source at the optical position of the SN with 4.5σ significance (Immler, Russell, & Brown 2009). Over the course of the Swift XRT observations, which lasted a month from discovery, the X-ray source continuously brightened from 8×10^{38} erg/s to 1.7×10^{39} erg/s (in the range 0.2-10 keV, Immler, Russell, & Brown 2009). During the same period no radio emission was detected at the SN position with 3σ upper limits of 0.35 mJy at a resolution of 0.38″ at 1.3 cm, and of 0.15 mJy at a resolution of 1.1″ at 3.5 cm (Stockdale et al. 2009).
   NED provides the velocity of the host galaxy corrected for Virgo infall, $v_{Virgo} = 1025 \pm 15$km s^{-1} (from Mould et al. 2000). Corresponding to a distance modulus $\mu = 30.74\pm0.15$ mag (d$\sim$14.0 Mpc) which will be used throughout this paper. The coordinates of SN 2009dd, measured on our astrometrically calibrated images on two different epochs, are $\alpha =$

$12^h05^m34^s.10 \pm 0^s.05$, $\delta = +50°32'19''.40 \pm 0''.05$ (J2000). The object is located in the galaxy inner region, $1''.5$ West and $4''$ South of the nucleus of NGC 4088. This position, slightly revised with respect to the previous determination (Cortini & Dimai 2009), corresponds to a linear distance of ∼0.3 kpc from the nucleus, deprojected as in Hakobyan et al. (2009).

The Galactic reddening toward NGC 4088 is E_g(B-V) = 0.02 mag (A_g(B) = 0.085 mag, Schlegel et al. 1998). In our best resolution optical spectra (cfr. Sect. 3.2.1), the interstellar Na ID ($\lambda\lambda$5890,5896) lines of the Galaxy are seen with average EW_g(NaID)∼0.13 Å. According to Turatto, Benetti, and Cappellaro (2003) this corresponds to a galactic reddening E_g(B-V)∼0.02 mag that considering the large uncertainties in the measurements and in the empirical method, is in agreement with the Schlegel et al. (1998) estimate. With the same method we estimate the reddening inside the parent galaxy. The corresponding interstellar Na ID components have an average equivalent width $EW_i(Na\ ID) \sim 2.70$ Å, providing an $E_i(B-V)$ ∼0.43 mag or $A_i(B)$ ∼1.81 mag. We should warn the reader that recently Poznanski et al. (2011) have suggested that Na ID lines in SN Ia spectra are poor tracers of dust extinction. Missing other more precise methods of determination of the reddening we have adopted a total reddening to SN 2009dd $E_{tot}(B-V)$ = 0.45 mag, consistent with the position of the SN inside the parent galaxy and what reported in Elias-Rosa et al. (2009).

To estimate the metallicity a reasonable assumption is to consider that the SN has the same metallicity of the closest HII region. Extracting the spectrum of the region close to SN from the latest, deep observation of SN 2009dd, we have determined the N2 index (Pettini & Pagel 2004) to be N2= −0.54. The relation (1) of Pettini & Pagel (2004) then provides the O abundances which turns out to be 12 + $log(O/H)$ = 8.59 ± 0.06 ± 0.41 (where the first error is statistical and the second one is the 95% spread of the N2 index calibration relation), close to the solar abundance (8.69, Asplund et al. 2009). Following López-Sánchez & Esteban (2010) this is equivalent to $Z \sim 0.019$.

2. SN 2007pk (Fig. 2), discovered in NGC 579 on 2007 November 10.31 UT, has been classified as a young "peculiar" type IIn SN resembling SN 1998S at early phases (Parisky et al. 2007). Immler et al. (2007) reported a bright X-ray source within $23''.5$ from the SN position. Inspection of the XRT raw image by Immler et al. (2007) indicated that some of the X-ray flux might be due to the SN, although the results were not conclusive due to the large point-spread-function of the XRT instrument ($18''$ half-power diameter at 1.5 keV). An X-ray flux of $(2.9 \pm 0.5) \times 10^{-13}$ erg cm^{-2} s^{-1} and a luminosity of $(1.7 \pm 0.3) \times 10^{40}$ erg s^{-1} have been calculated. No radio emission has been detected at VLA in the 8.46 GHz band (Chandra & Soderberg 2007).

NED provides a recession velocity of NGC 579 corrected for Virgo infall of $v_{Virgo} = 5116 \pm 16$ km s^{-1} (from Mould et al. 2000). and a consequently we obtain a distance modulus $\mu = 34.23 \pm 0.15$ mag.

The coordinates of SN 2007pk, $\alpha = 01^h31^m47^s.07 \pm 0^s.04$ and $\delta = +33°36'54''.70 \pm 0''.04$ (J2000), measured on our astrometrically calibrated images on three different epochs, are in good agreement ($\Delta(\delta) = 0''.6$) with those provided by Parisky et al. (2007). The object is located in an inner region of the Spiral parent galaxy, $7''.4$ East and $1''.6$ South (slightly revised with respect to the determination of Parisky
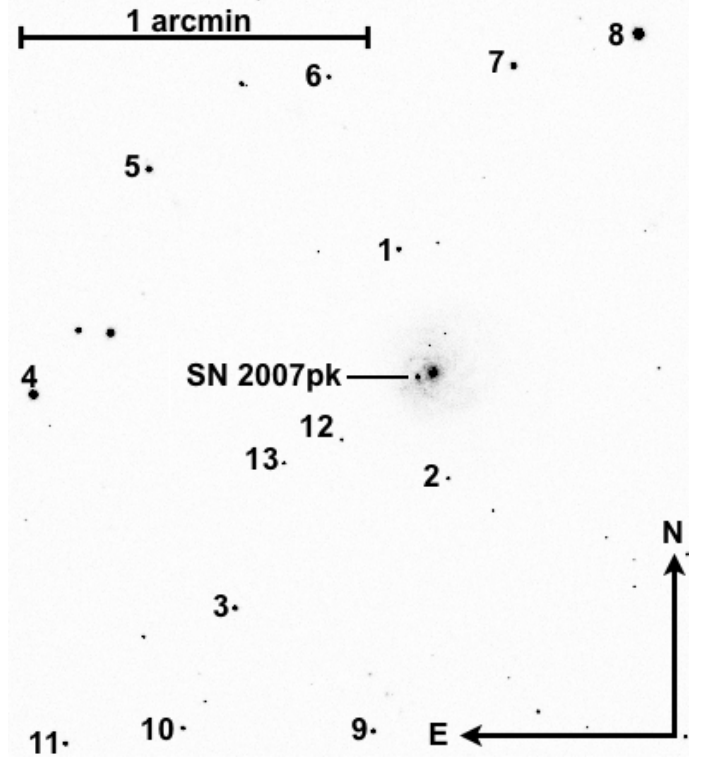

Fig. 2. R band image of SN 2007pk in NGC 579 obtained with NOT+ALFOSC on January 11th, 2008. The sequence of stars in the field used to calibrate the optical magnitude of the 2007pk is indicated.

et al. 2007) from the nucleus of NGC 579. The position of SN corresponds to a linear deprojected distance of ∼2.5 kpc from the nucleus (cfr. Hakobyan et al. 2009).

The Galactic reddening toward NGC 579 was estimated as $E_g(B-V)$ = 0.05 mag (A_g(B) = 0.22 mag, Schlegel et al. 1998). We have measured the intensity of the interstellar Na ID lines of the Galaxy in our best resolution spectra, finding an average of $EW_g(Na\ ID)$ ∼0.57 Å. This corresponds to a galactic reddening of $E_g(B-V)$ ∼0.09 mag (A_g(B) ∼0.38 mag) according to Turatto, Benetti, and Cappellaro (2003), 1.8 times larger than the previous estimate but still within the large uncertainty of the method. In analogy we estimated the reddening inside the parent galaxy with the interstellar Na ID components within the host galaxy. The derived $EW_i(NaID)$ ∼0.33 Å corresponds to reddening $E_i(B-V)$ ∼0.05 mag or $A_i(B)$ ∼0.22 mag, about three time less than the estimate by Pritchard et al. (2012). Throughout this work we have adopted a total reddening to SN 2007pk $E_{tot}(B-V)$ = 0.10 mag.

As for SN 2009dd we have measured the emission lines of the region adjacent to the SN along the slit. We determined the index $N2 = -0.70$ corresponding to 12 + $log(O/H)$ = 8.50 ± 0.05 ± 0.41, again nearly solar.

3. SN 2010aj was discovered in MGC-01-32-035 by Newton et al. (2010) on 2010 March 12.39 UT and classified it as a young type II SN resembling the type IIP SN 2006bp near maximum brightness (Cenko et al. 2010). The recession velocity of MGC-01-32-035 corrected for the Virgo infall is $v_{Virgo} = 6386 \pm 20$ km s^{-1} (Mould et al. 2000, from NED), the distance modulus is $\mu = 34.71 \pm 0.15$ mag.
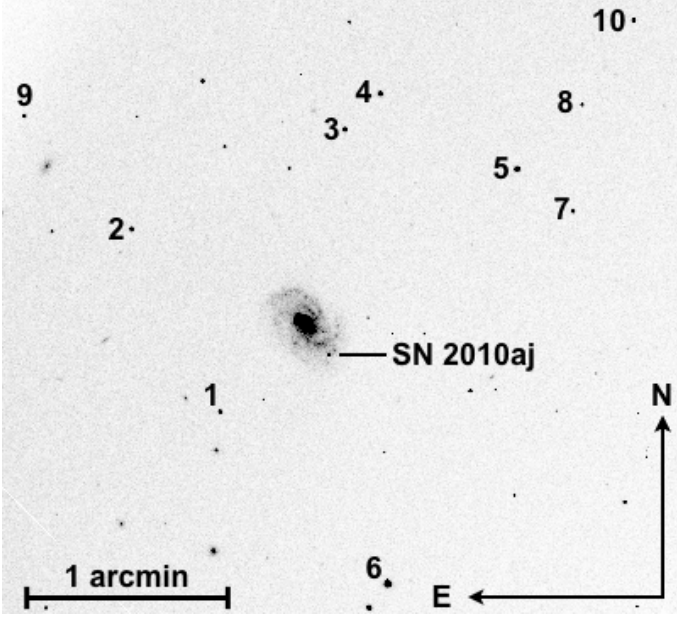
Fig. 3. R band image of SN 2010aj in MGC-01-32-035 obtained with TNG+DOLORES on May 22th, 2010. The sequence of stars in the field used to calibrate the optical and NIR magnitudes of SN 2010aj is indicated.

Fig. 4. R band image of SN 1995ad in NGC 2139 obtained with ESO 3.6m+EFOSC1 on December 29th, 1995. The sequence of stars in the field used to calibrate the optical magnitudes of SN 1995ad is indicated.

The coordinates of SN 2010aj have been measured on our images at $\alpha = 12^h40^m15^s.16 \pm 0^s.05$, $\delta = -09°18'14''.30 \pm 0''.05$ (J2000). The object is located $12''.4$ West and $11''.7$ South of the centre of the SABbc: parent galaxy, (Fig. 3). The SN is centred on an H II region that becomes dominant after 350d as clearly seen from the SN spectral evolution in Sec. 4. The linear deprojected distance is ~ 7.2 kpc from the nucleus.

The Galactic reddening in the direction to MGC -01-32-035 was estimated as $E_g(B - V) = 0.036$ mag ($A_g(B) = 0.148$ mag, Schlegel et al. 1998). The available spectra do not show neither the Na ID lines of the parent galaxy nor those of the Galactic component. Throughout this paper, we will adopt a total reddening to SN 2010aj of $E_{tot}(B - V) = E_g(B - V) = 0.036$ mag, entirely due to the Galaxy.

Also for this SNe we measured the N2 index, $N2(SN\ 2010aj) = -0.47$, providing a metallicity of $12 + log(O/H) = 8.63 \pm 0.06 \pm 0.41$, corresponding to $Z \sim 0.02$.

4. SN 1995ad (Fig. 4) was discovered by Evans et al. (1995) on 28.8 UT of September in NGC 2139. Based on a spectrum collected the day after with the ESO 1.5-m telescope in La Silla it was classified as a type II close to maximum because of broad P-Cygni profiles of Balmer and He I lines lying on a blue continuum ($T_{bb} \sim 13000$ K, Evans et al. 1995) . NED provides a heliocentric radial velocity of NGC 2139 corrected for the Virgo Infall of $v_{Virgo} = 1674 \pm 14$ km s^{-1}, from which we infer a distance modulus $\mu = 31.80 \pm 0.15$ mag.

The coordinates of the SN, measured on our astrometrically calibrated images on two different epochs, are $\alpha = 06^h01^m06^s.21 \pm 0^s.05$ and $\delta = -23°40'28''.90 \pm 0''.05$ (J2000). The object is located in an arm of the host galaxy, $25''$ West and $5''$ South of the nucleus of NGC 2139. This position, slightly revised with respect to a previous determi-
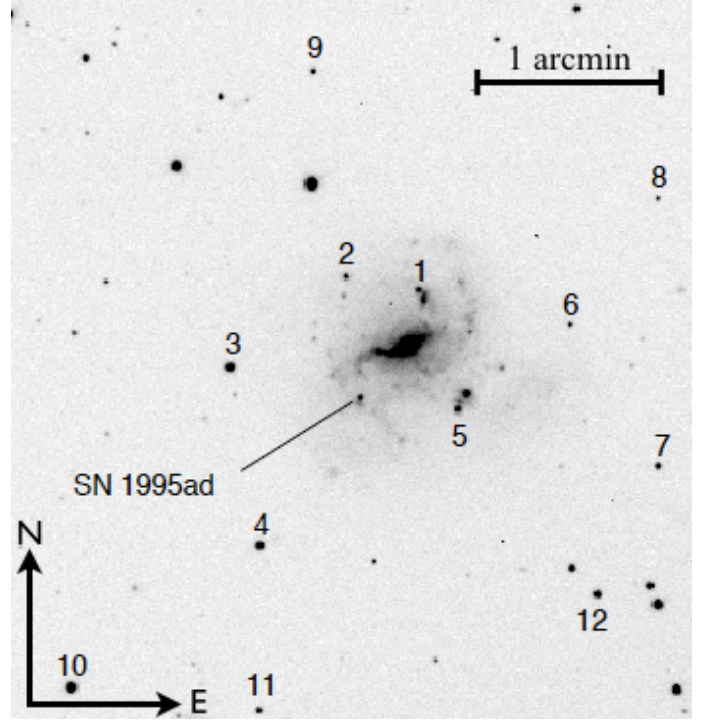
nation (McNaught & Pollas 1995), corresponds to a deprojected distance of ~ 2.8 kpc from the nucleus.

The Galactic reddening has been estimated as $E_g(B - V) = 0.035$ mag (i.e. $A_g(B) = 0.145$ mag, Schlegel et al. 1998). The Na ID interstellar lines associated to the parent galaxy are not visible in the SN spectra. Therefore, hereafter, we consider only the Galactic contribution.

To obtain the metallicity of the environment of this SN, we analysed the spectra obtained at the ESO1.5m telescope on February 19 and 20, 1996 because of the better resolution than the latest available spectra. We measured the O3N2 and N2 indices (Pettini & Pagel 2004) of an H II region close to the SN. The average relations then provide $12 + log(O/H) = 8.60 \pm 0.05 \pm 0.41$ corresponding to $Z \sim 0.02$.

5. SN 1996W (Fig. 5) was discovered on April 10 UT and confirmed the following night at the Beijing Astronomical Observatory (BAO) (Li et al. 1996) as a type II SN soon after the explosion, showing a blue continuum with strong and broad Hα ($v \sim 14300$ km s^{-1}) and Hβ. The recession velocity of NGC 4027 corrected for Virgo infall is $v_{Virgo} = 1779 \pm 29$ km s^{-1}(Mould et al. 2000, from NED), corresponding to a distance modulus $\mu = 31.93 \pm 0.15$ mag.

The coordinates of SN 1996W, measured on our astrometrically calibrated images on two different epochs, are: $\alpha = 11^h59^m28^s.98 \pm 0^s.05$ and $\delta = -19°15'21''.90 \pm 0''.05$ (J2000). The object is located in an arm of the host galaxy, $17''$ West and $34''$ North of the nucleus of the parent galaxy NGC 4027. This position, slightly revised with respect to previous determination (Suntzeff et al. 1996), corresponds to a deprojected distance of ~ 3.0 kpc from the nucleus.

The Galactic reddening has been estimated as $E_g(B - V) = 0.044$ mag ($A_g(B) = 0.145$ mag Schlegel et al. 1998). In the spectra of SN 1996W the absorption features due to in-
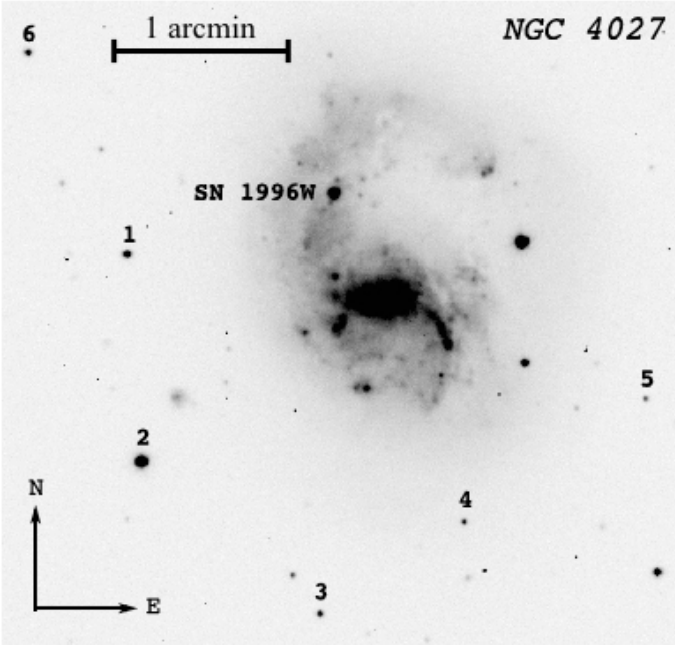
Fig. 5. R band image of SN 1996W in NGC 4027 obtained with the Dutch 0.9m telescope on May 13th, 1996. The local sequence of stars used to calibrate the optical magnitude is indicated.

terstellar Na ID lines both from our Galaxy and of the host galaxy have been identified, suggesting Galactic reddening $E_g(B - V) \sim 0.05$ mag. The parent galaxy reddening is $E_i(B - V) = 0.187$ mag ($A_i(B) = 0.77$ mag), which provides a total extinction of $E_{tot}(B - V) = 0.23$ mag ($A_{tot}(B)=0.95$ mag).

For the metallicity of the underlying H II region as representative of the metallicity of the SN environment, we obtained an oxygen abundance of $12 + log(O/H) = 8.60 \pm 0.06 \pm 0.41$, close to the solar value and equivalent to $Z \sim 0.02$.

3. Photometry

3.1. Data summary

Optical observations of SNe 2009dd, 2007pk, 2010aj, 1995ad and 1996W were obtained with ground based telescopes and the SWIFT satellite (see Table 1).

Observations were reduced following standard procedures in the IRAF[1] environment. Instrumental magnitudes were measured on the final images including overscan correction, bias subtraction, flat field correction and trimming.

Photometric zero points and colour terms were computed for all photometric nights through observations of Landolt standard fields (Landolt 1992). The average magnitudes of the local sequence stars were computed and used to calibrate the photometric zero points for the non-photometric nights. Magnitudes of the local sequence stars are reported in Tabs. A.1, A.2, A.3, A.4 & A.5 along with their r.m.s. (in brackets). The calibrated optical magnitudes of the SNe are reported in Tabs. 2, 3, 4, 5 & 6.

The magnitudes of the I-band filter of the NOT have been calibrated as Cousin I. For the LT Sloan photometry we subse-

quently applied an *S*-correction (Stritzinger et al. 2002; Pignata et al. 2004) to report the SN magnitudes to the standard Johnson-Cousins photometric system, finding an average correction of $\Delta U \sim 0.04$, $\Delta R \sim 0.01$ and $\Delta I \sim -0.10$. Note that the i-band filter used at the 2.56-m Nordic Optical Telescope (NOT) is an interference filter with central wavelength 7970 Å, slightly different from the classical Gunn or Cousins I and more similar to Sloan i. In our analysis, however, it was calibrated as Cousins I. In the case of SN 2009dd the discovery magnitude reported in Cortini & Dimai (2009) has been revised and reported as R band in Tab. 2.

Swift U, B, V aperture magnitudes were transformed to Johnson system through the colour transformations by Li et al. (2006). After comparison with optical ground-based data, offsets were applied when necessary (cfr. Sect. 3.2). The magnitudes of the SNe were obtained through a point spread function (PSF) fitting sometimes applied after template subtraction, depending on the background complexity and the availability of suitable template images. The uncertainties reported for each optical band in Tabs. 2, 3, 4, 5 & 6 were estimated by combining in quadrature the errors of photometric calibration and the error of PSF fitting through artificial star (i.e. at late time are upper limits for the error estimates). Limiting magnitudes computed with artificial stars in regions of similar background to those of the SNe are reported when the objects were not detected. Only significant magnitude limits are presented in Figs. 6, 7, 8, 9 & 10.

The NIR images of the SN fields were obtained combining several sky-subtracted, dithered exposures. Photometric calibration was achieved relative to the 2MASS photometry of the same local sequence stars as used for the optical calibration. The NIR magnitudes of the sample are listed in the same tables of the optical magnitudes with relative errors. NIR photometry was obtained just at a single epoch for SNe 2009dd, 2010aj and 1995ad. In the case of SN 2009dd the K' filter was used but was calibrated as K band.

Ultraviolet (uvw2, uvm2, uvw1; see Poole et al. 2008) observations, obtained by UVOT on board of the SWIFT satellite are available for twenty-four epochs in a period of 160d in the case of SN 2009dd and for ten epochs in 23d for SN 2007pk. We reduced these data using the HEASARC[2] software. For each epoch all images were co-added, and then reduced following the guidelines presented by Poole et al. (2008). Aperture magnitudes are reported in the same tables of the optical.

The follow-up coverage of individual SNe is scanty and incomplete. However, we argue that these objects form a fairly homogenous group and so, taken together, they provide a fairly complete picture of the photometric evolution of this type of SNe.

3.2. Bright light curves

In this Section we present the main photometric information for the full SN sample (some of that are reported in Tab. 7).

3.2.1. SN 2009dd

The optical monitoring campaign of SN 2009dd started on April 14, 2009, the day after the discovery, and continued until October 2010. Because of the location of the SN very close to the galaxy nucleus, the optical photometric measurements of

---

Table 1. Instrumental configurations used for the 5 SN monitoring campaigns.

Telescope	Primary mirror m	Camera	Array	CCD	pixel scale arcsec/pix	field of view arcmin
Ekar	1.8	AFOSC	1024 x 1024	TK1024AB	0.46	8.1
	1.8	TL512†	512 x 512	TK512	0.34	
		B&C†	576 x 384	TH7882	0.29	
TNG	3.6	DOLORES	2048 x 2048	EEV 42-40	0.25	8.6
		NICS	1024 x 1024	HgCdTe Hawaii	0.25	
LT	2.0	RATcam	2048 x 2048	EEV 42-40	0.13	4.6
NOT	2.5	ALFOSC	2048 x 2048	EEV 42-40	0.19	6.4
CAHA	2.2	CAFOS	2048 x 2048	SITe	0.53	16.0
SWIFT	0.3	UVOT	2048 x 2048	intensified CCD	0.48	17.0
NTT	3.6	EFOSC2	2048 x 2048	Loral/Lesser	0.16	5.2
		SOFI	1024 x 1024	Hawaii HgCdTe	0.29	
ESO 1.5	1.5	B&C	2048 x 2048	Loral	0.82	8.0
MPG-ESO 2.2	2.2	EFOSC2	1024 x 1024	THX31156	0.34	5.7
ESO 3.6	3.6	EFOSC1	512 x 512	Tek512	0.61	3.6 x 5.76
Dutch	0.9	CCD phot.	512 x 512	Tek512	0.48	3.8
Danish	1.5	DFOSC	2052 x 2052	W11-4 Loral/Lesser	0.39	13.3

Ekar = Copernico Telescope (Mt. Ekar, Asiago, Italy); TNG = Telescopio Nazionale Galileo (La Palma, Spain); LT = Liverpool Telescope (La Palma, Spain); NOT = Nordic Optical Telescope (La Palma, Spain); Caha = Calar Alto Observatory 2.2m Telescope (Sierra de los Filabres, Andalucia, Spain); SWIFT by NASA; NTT = New Technology Telescope (La Silla, Chile); ESO 1.5 = ESO 1.5m Telescope (La SIlla, Chile); MPG-ESO 2.2 = MPG-ESO 2.2m Telescope (La Silla, Chile); ESO 3.6 = ESO 3.6m Telescope (La SIlla, Chile); Dutch = Dutch 0.9m Telescope (La SIlla, Chile); Danish = Danish 1.5m Telescope (La Silla, Chile)
† Instruments used until 1998

Table 2. Ultraviolet, optical and infrared photometry of SN 2009dd.

Date yy/mm/dd	JD (+2400000)	uvw2	uvm2	uvw1	U	B	V	R	I	J	H	K'	Inst.†
09/04/13	54935.61	-	-	-	-	-	-	13.88 (.10)	-	-	-	-	99
09/04/14	54936.67	-	-	-	14.74 (.02)	15.07 (.06)	14.87 (.06)	14.60 (.06)	14.62 (.04)	-	-	-	1
09/04/15	54936.63	-	-	-	-	-	-	-	-	14.32 (.04)	14.25 (.05)	14.12 (.06)	2
09/04/15	54937.12	16.97 (.07)	16.88 (.05)	15.66 (.05)	14.76 (.09)	15.20 (.08)	14.85 (.08)	-	-	-	-	-	5
09/04/16	54938.40	-	-	-	14.86 (.03)	15.27 (.05)	14.83 (.06)	14.62 (.06)	14.64 (.05)	-	-	-	4
09/04/17	54939.08	17.44 (.13)	-	16.00 (.04)	14.96 (.06)	15.31 (.06)	14.76 (.06)	-	-	-	-	-	5
09/04/19	54940.87	17.25 (.08)	17.39(.09)	-	15.19 (.05)	15.32 (.06)	14.83 (.04)	-	-	-	-	-	5
09/04/21	54943.00	17.53 (.07)	17.51 (.09)	16.63 (.08)	15.49 (.08)	15.44 (.08)	14.90 (.04)	-	-	-	-	-	5
09/04/25	54946.62	18.10 (.11)	18.01 (.10)	16.82 (.09)	16.06 (.06)	15.61 (.05)	14.90 (.04)	-	-	-	-	-	5
09/05/10	54961.54	19.55 (.08)	19.11 (.08)	-	17.18 (.06)	16.31 (.05)	15.20 (.04)	-	-	-	-	-	5
09/05/11	54963.29	-	19.46 (.09)	-	-	-	-	-	-	-	-	-	5
09/05/19	54971.58	-	-	-	17.99 (.10)	16.87 (.02)	15.48 (.01)	14.67 (.04)	14.57 (.05)	-	-	-	2
09/07/05	55017.50	20.17 (.15)	20.18 (.12)	19.29 (.10)	19.21 (.06)	17.83 (.05)	16.15 (.04)	-	-	-	-	-	5
09/07/15	55028.21	-	-	19.52 (.11)	-	-	-	-	-	-	-	-	5
09/07/16	55028.54	-	-	-	19.72 (.06)	-	-	-	-	-	-	-	5
09/07/19	55032.12	-	-	19.91 (.13)	-	-	-	-	-	-	-	-	5
09/07/20	55032.54	> 20.1	-	> 20.1	19.92 (.13)	-	-	-	-	-	-	-	5
09/07/20	55033.41	-	-	-	20.01 (.13)	18.21 (.09)	16.28 (.06)	15.45 (.05)	15.17 (.04)	-	-	-	2
09/07/21	55034.31	-	-	-	-	18.20 (.06)	16.35 (.01)	15.47 (.02)	15.14 (.02)	-	-	-	3
09/07/23	55036.39	-	-	-	-	18.36 (.02)	16.38 (.01)	15.53 (.05)	15.19 (.07)	-	-	-	3
09/07/26	55038.62	-	> 20.4	-	-	-	-	-	-	-	-	-	5
09/07/27	55039.62	-	-	> 20.2	-	-	-	-	-	-	-	-	5
09/07/30	55042.40	-	-	-	-	18.81 (.06)	16.88 (.05)	15.95 (.05)	15.70 (.07)	-	-	-	4
09/08/02	55046.00	> 20.3	> 20.3	-	-	-	-	-	-	-	-	-	5
09/08/03	55046.75	-	> 20.2	-	-	-	-	-	-	-	-	-	5
09/08/09	55052.50	> 20.4	-	-	> 19.2	-	-	-	-	-	-	-	5
09/08/12	55056.50	-	-	-	-	19.63 (.04)	17.79 (.09)	16.74 (.02)	16.66 (.05)	-	-	-	1
09/08/20	55064.36	-	-	-	-	19.73 (.20)	17.92 (.03)	16.84 (.08)	16.72 (.02)	-	-	-	3
09/09/04	55079.31	-	-	-	-	-	18.20 (.04)	17.04 (.19)	16.99 (.20)	-	-	-	4
09/09/13	55088.50	-	-	> 20.3	-	-	-	-	-	-	-	-	5
09/09/14	55089.50	-	-	-	> 19.2	-	-	-	-	-	-	-	5
09/09/16	55091.58	-	> 20.4	-	-	-	-	-	-	-	-	-	5
09/09/21	55095.46	-	-	> 20.5	> 19.3	-	-	-	-	-	-	-	5
09/11/19	55155.65	-	-	-	-	20.82 (.03)	18.92 (.10)	17.76 (.09)	17.36 (.06)	-	-	-	4
09/11/21	55157.70	-	-	-	-	20.93 (.04)	18.98 (.15)	17.83 (.10)	17.44 (.04)	-	-	-	2
10/01/19	55216.20	-	-	-	-	-	19.73 (.20)	18.83 (.20)	-	-	-	-	3
10/05/17	55334.43	-	-	-	-	> 20.7	> 20.1	> 19.8	> 19.3	-	-	-	2
10/10/25	55495.67	-	-	-	-	> 20.7	> 20.6	> 19.9	> 20.0	-	-	-	4

† 1 = NOT, 2 = TNG, 3 = Ekar, 4 = CAHA, 5 = Swift, 99 = CBET 1764 (revised measure) where instruments are coded as in Tab.1.

Table 3. Ultraviolet and optical photometry of SN 2007pk.

Date yy/mm/dd	JD (+2400000)	uvw2	uvm2	uvw1	U	B	V	R	I	Inst.†
07/11/10	54415.30	-	-	-	-	-	-	17.00 (-)	-	99
07/11/11	54416.40	-	-	-	-	16.25 (.02)	16.37 (.02)	16.37 (.03)	16.45 (.03)	1
07/11/12	54417.50	-	-	-	-	16.00 (.15)	16.17 (.17)	16.20 (.18)	15.89 (.19)	1
07/11/13	54417.66	-	-	14.50 (.04)	-	-	-	-	-	6
07/11/14	54418.65	14.54 (.06)	14.46 (.06)	14.64 (.05)	15.13 (.05)	16.05 (.06)	16.15 (.04)	-	-	6
07/11/15	54420.24	14.92 (.05)	14.69 (. 05)	14.78 (.04)	15.17 (.05)	16.07 (.06)	16.09 (.04)	-	-	6
07/11/16	54420.66	15.14 (.06)	14.84 (. 06)	14.87 (.05)	15.19 (.05)	16.08 (.06)	16.09 (.04)	-	-	6
07/11/16	54421.50	-	-	-	15.20 (.04)	16.14 (.04)	16.20 (.03)	15.88 (.04)	15.99 (.03)	2
07/11/17	54421.68	15.45 (.06)	15.11 (.06)	15.08 (.05)	15.22 (.06)	16.14 (.06)	16.23 (.05)	-	-	6
07/11/20	54425.08	16.03 (.06)	15.73 (.06)	15.48 (.05)	-	-	-	-	-	6
07/11/25	54429.65	16.91 (.07)	16.74 (.07)	16.32 (.08)	15.69 (.06)	16.28 (.06)	16.23 (.04)	-	-	6
07/11/29	54433.91	17.85 (.09)	17.58 (.09)	17.02 (.08)	16.13 (.06)	16.42 (.07)	16.27 (.05)	-	-	6
07/12/02	54436.96	18.44 (.10)	18.59 (.14)	17.64 (.09)	16.45 (.06)	16.57 (.06)	16.27 (.05)	-	-	6
07/12/04	54439.39	-	-	-	-	16.62 (.24)	16.31 (.24)	16.14 (.27)	16.01 (.29)	1
07/12/06	54440.81	19.01 (.10)	-	18.07 (.10)	16.61 (.06)	16.69 (.07)	16.32 (.05)	-	-	6
07/12/08	54443.50	-	-	-	16.65 (.03)	16.86 (.02)	16.43 (.02)	16.23 (.021)	16.00 (.02)	3
07/12/13	54448.40	-	-	-	-	-	16.51 (.02)	16.38 (.09)	16.00 (.04)	1
07/12/14	54449.50	-	-	-	17.29 (.03)	17.21 (.03)	16.62 (.03)	16.36 (.03)	16.01 (.03)	3
07/12/17	54451.65	-	-	-	17.39 (.06)	17.27 (.07)	16.68 (.06)	-	-	6
07/12/24	54459.50	-	-	-	18.02 (.10)	17.65 (.04)	16.82 (.03)	16.41 (.03)	16.19 (.02)	3
07/12/27	54462.01	-	-	-	18.20 (.08)	17.78 (.08)	16.95 (.05)	-	-	6
07/12/28	54463.29	-	-	-	-	17.92 (.12)	16.96 (.10)	16.53 (.05)	16.26 (.04)	1
08/01/08	54474.09	-	-	-	18.52 (.08)	18.11 (.10)	17.09 (.06)	-	-	6
08/01/09	54475.39	-	-	-	-	18.14 (.23)	17.13 (.23)	16.63 (.18)	-	1
08/01/11	54477.40	-	-	-	18.73 (.05)	18.34 (.03)	17.19 (.02)	16.69 (.03)	16.40 (.03)	4
08/01/28	54494.36	-	-	-	-	18.49 (.93)	17.46 (.16)	17.04 (.16)	16.69 (.13)	1
08/09/04	54714.64	-	-	-	-	-	> 19.8	>19.6	> 19.4	2
08/09/14	54723.69	-	-	-	-	>19.8	> 20.1	>19.6	-	5

† 1 = Ekar, 2 = TNG, 3 = LT, 4 = NOT, 5 = CAHA, 6 = Swift, 99 = CBET 1129, where instruments are coded as in Tab.1.

SN 2009dd were performed using the template subtraction technique (Tab. 2).

By comparing the space and the ground-based UBV magnitudes, computed interpolating the light curves with low-order polynomials at corresponding epochs, we found average differences (ground–space) $\Delta U \sim 0.20 \pm 0.03$, $\Delta B \sim 0.06 \pm 0.03$, $\Delta V \sim 0.10 \pm 0.03$. These corrections have been applied to all UVOT magnitudes and the resulting magnitude values are reported in Tab. 2.

In Fig. 6 the uvw2, uvm2, uvw1, U, B, V, R, I light curves of SN 2009dd are plotted; where the single NIR epoch was not reported. No band shows a rise to the peak. Lacking any other constraints, we have adopted JD 2454925.5±5.0 (April 04 UT) as the epoch of the explosion, which is in agreement with that deduced from the comparison of the early spectra of SN 2009dd with a library of SN spectra performed with the *GELATO* code (Harutyunyan et al. 2008).

Assuming the distance and extinction discussed in Sect. 2, we find $M_U^{max} \leq -18.22 \pm 0.25$, $M_B^{max} \leq -17.61 \pm 0.27$, $M_V^{max} \leq -17.46 \pm 0.23$, $M_R^{max} \leq -17.38 \pm 0.21$ and $M_I^{max} \leq -17.09 \pm 0.18$, where the reported errors include the uncertainties on the distance modulus adopted and measurement errors.

An initial rapid decline is visible from U to V during the first 30 days ($\Delta m(B) \sim 1.2$ mag). It was followed by a plateau lasting about 50–70 days, visible from V to I bands. The plateau luminosity of SN 2009dd was more luminous ($m_V \sim 16$, corresponding to $M_V \sim -16.8$ compared to an average of $M_B \sim -15.5$ and $M_V \sim -15.9$ for SNe IIP, Patat et al. 1994; Li et al. 2011) than for normal SNIIP, but fainter than the luminous IIPs 1992H ($M_V \sim -17.3$, Clocchiatti et al. 1996), 2007od ($M_V \sim -17.4$, Inserra et al. 2011) and 2009bw ($M_V \sim -17.2$, Inserra et al.
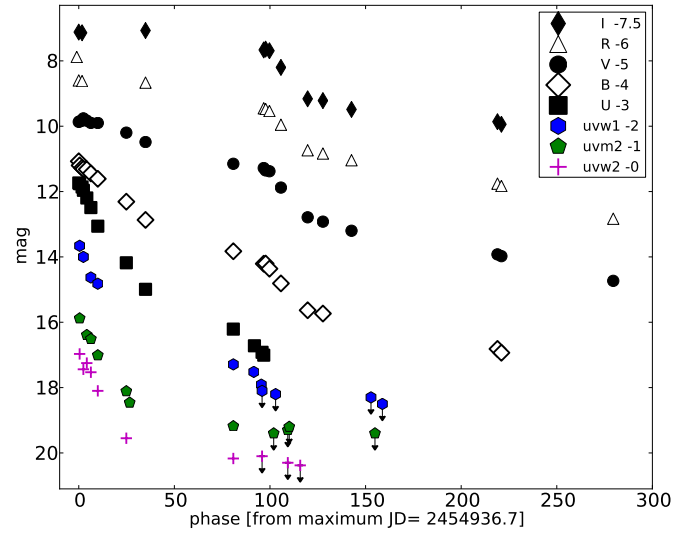

Fig. 6. Synoptic view of the light curves of SN 2009dd in uv and optical bands. Magnitude shifts for the different bands are in the legenda.

2012a). The post plateau decline visible in the BVRI light curves introduces the nebular phase. The drop in magnitude between the photospheric and the nebular phase is $\Delta m(V) \sim 1.4$ mag in ~ 20d in the V band, which is somewhat lower than the value of 2 mag in normal SNe IIP. The late decline rates in the various bands are similar. During the 120–280 d interval the V band decline rate

Table 4. Optical and infrared photometry of SN 2010aj.

Date yy/mm/dd	JD (+2400000)	U	B	V	R	I	J	H	K	Inst.†
10/03/12	55268.50	-	-	-	17.1 (-)	-	-	-	-	99
10/03/13	55269.50	-	-	-	17.0 (-)	-	-	-	-	99
10/03/24	55280.50	-	18.20 (.06)	17.75 (.03)	17.55 (.03)	17.34 (.05)	-	-	-	1
10/03/27	55282.95	-	18.30 (.04)	17.78 (.03)	17.57 (.02)	17.33 (.04)	-	-	-	1
10/04/16	55303.50	-	18.72 (.13)	18.16 (.03)	17.82 (.03)	17.45 (.06)	-	-	-	2
10/04/18	55305.50	-	-	-	-	-	19.42 (.04)	20.19 (.08)	20.21 (.05)	2
10/04/24	55311.52	-	19.30 (.11)	18.29 (.04)	17.83 (.03)	17.54 (.03)	-	-	-	3
10/05/05	55321.90	20.21 (.17)	19.55 (.09)	18.47 (.06)	17.99 (.03)	17.85 (.03)	-	-	-	1
10/05/07	55324.00	20.27 (.21)	19.65 (.12)	18.62 (.07)	18.11 (.04)	17.81 (.06)	-	-	-	1
10/05/18	55334.95	20.36 (.25)	19.90 (.12)	18.83 (.07)	18.24 (.05)	18.13 (.08)	-	-	-	1
10/05/22	55339.38	20.44 (.23)	19.97 (.10)	18.93 (.07)	18.32 (.05)	18.23 (.06)	-	-	-	3
10/05/26	55342.92	20.51 (.23)	20.30 (.15)	19.17 (.07)	18.53 (.06)	18.43 (.06)	-	-	-	1
10/06/09	55356.93	-	22.82 (.24)	-	21.01 (.19)	20.74 (.30)	-	-	-	1
10/06/12	55359.89	-	>20.7	21.91 (.30)	21.16 (.28)	21.03 (.20)	-	-	-	1
10/06/16	55363.94	-	>20.7	22.28 (.21)	21.18 (.11)	21.11 (.11)	-	-	-	1
10/06/17	55365.14	-	-	>20.6	> 20.2	>20.0	-	-	-	2
10/06/21	55368.91	-	>20.5	>20.5	21.25 (.14)	21.17 (.12)	-	-	-	1
10/06/24	55371.91	-	>20.7	>20.7	21.58 (.04)	21.31 (.14)	-	-	-	1
10/07/08	55386.46	-	>20.9	>20.6	>20.1	>20.4	-	-	-	3
11/01/01	55563.31	-	>20.5	>20.6	>20.2	>20.0	-	-	-	2
11/01/25	55587.30	-	>20.6	>20.6	>20.3	>20.5	-	-	-	2

† 1 = LT, 2 = NTT, 3 = TNG, 99 = CBET 2201, where instruments are coded as in Tab.1.

Table 5. Optical and infrared magnitudes of SN 1995ad and assigned errors.

Date yy/mm/dd	JD (+2400000)	B	V	R	I	J	H	K	Inst.†
95/09/22	49983.29	-	-	15.70 (-)	-	-	-	-	98
95/09/28	49989.30	-	14.25 (.25)	-	-	-	-	-	99
95/09/29	49989.80	14.77 (.20)	14.73 (.15)	14.67 (.15)	-	-	-	-	1
95/10/02	49992.88	15.17 (.01)	15.03 (.01)	14.85 (.01)	14.75 (.01)	-	-	-	2
95/10/14	50004.90	-	15.29 (.02)	14.98 (.02)	-	-	-	-	2
95/11/24	50045.53	16.90 (.03)	15.81 (.02)	15.30 (.02)	-	-	-	-	3
95/12/26	50077.71	-	-	16.92 (.03)	-	-	-	-	4
95/12/26	50077.73	19.79 (.01)	17.96 (.06)	16.93 (.03)	16.37 (.02)	-	-	-	4
96/12/29	50080.74	-	18.00 (.09)	17.07 (.07)	-	-	-	-	2
96/01/17	50100.42	19.83 (.30)	18.32 (.19)	17.35 (.12)	-	-	-	-	3
96/01/19	50102.45	19.91 (.25)	18.35 (.12)	17.38 (.10)	16.89 (.10)	-	-	-	5
96/02/18	50131.63	19.94 (.10)	18.59 (.05)	-	-	-	-	-	4
96/02/22	50135.65	20.08 (.30)	18.51 (.15)	17.61 (.10)	17.15 (.10)	-	-	-	5
96/02/23	50136.65	19.96 (.30)	18.53 (.15)	17.61 (.10)	17.18 (.10)	-	-	-	5
96/04/20	50193.52	20.16 (.35)	19.14 (.20)	18.20 (.15)	17.76 (.15)	-	-	-	5
96/04/21	50194.55	-	19.07 (.20)	18.19 (.15)	17.75 (.15)	-	-	-	5
96/04/29	50203.50	-	-	-	-	17.69 (.20)	17.67 (.30)	17.13 (.50)	2
96/05/14	50217.50	>20.5	19.54 (.25)	18.58 (.20)	-	-	-	-	5
96/10/02	50358.87	>23.0	22.42 (.55)	20.21 (.15)	-	-	-	-	6
96/11/19	50406.85	-	-	20.79 (.40)	-	-	-	-	5
97/02/19	50489.53	-	-	>21.5	-	-	-	-	2

† 1 = ESO 1.5, 2 = ESO 3.6 , 3 = Ekar, 4 = MPG-ESO 2.2, 5 = Dutch, 6 = Danish, 98 = IAUC 6852, 99 = IAUC 6239, where instruments are coded as in Tab.1.

is 1.15 mag $(100d)^{-1}$, marginally higher than the decline rate expected from ^{56}Co to ^{56}Fe decay (0.98 mag $(100d)^{-1}$) in case of complete γ-ray trapping.

3.2.2. SN 2007pk

The optical photometric monitoring of SN 2007pk started on November 11th, 2007 and continued until January 2008. SN observations during the nebular phase turned out with only upper limits, preventing the determination of the ^{56}Ni mass. Because of the proximity to the nucleus of the host galaxy and a nearby HII region, also in this case the optical photometric measurements of SN 2007pk were performed using the template subtraction technique. The Swift data have been treated as for SN 2009dd. The comparison of space and ground-based photometry at corresponding epochs pointed out systematic average differences (ground–space) $\Delta(U) \sim 0.20 \pm 0.05$, $\Delta(B) \sim 0.06 \pm 0.02$, $\Delta(V) \sim 0.07 \pm 0.03$. As before, Tab. 3 reports the corrected mag-

Table 6. Optical magnitudes of SN 1996W and assigned errors.

Date yy/mm/dd	JD (+2400000)	U	B	V	R	I	Inst.†
96/04/10	50183.50	-	-	16.00 (-)	-	-	6
96/04/11	50184.50	-	-	16.00 (-)	-	-	6
96/04/13	50186.60	-	-	15.10 (-)	-	-	6
96/04/16	50190.40	-	15.53 (.02)	15.18 (.02)	14.77 (.04)	-	1
96/04/18	50192.40	-	15.51 (.02)	15.26 (.01)	14.79 (.01)	-	1
96/04/18	50192.41	-	-	15.26 (.01)	-	-	1
96/04/19	50192.50	-	15.45 (.03)	15.15 (.01)	14.77 (.01)	14.60 (.02)	2
96/04/20	50193.50	-	15.51 (.03)	15.12 (.01)	14.75 (.01)	14.59 (.02)	2
96/04/25	50198.54	15.21 (.30)	15.53 (.15)	15.20 (.10)	14.79 (.10)	14.62 (.15)	3
96/05/09	50212.50	-	15.89 (.20)	15.22 (.15)	14.74 (.10)	14.49 (.15)	3
96/05/11	50215.63	-	15.95 (.20)	15.24 (.15)	14.76 (.10)	14.49 (.15)	3
96/05/13	50217.50	16.75 (.05)	16.12 (.03)	15.25 (.03)	14.79 (.03)	14.49 (.03)	2
96/05/14	50218.50	16.82 (.07)	16.15 (.03)	15.26 (.03)	14.79 (.03)	14.50 (.04)	2
96/05/19	50222.54	16.90 (.03)	16.32 (.01)	15.31 (.01)	14.79 (.01)	14.49 (.02)	4
96/12/15	50432.81	-	19.24 (.13)	18.34 (.12)	17.38 (.06)	17.02 (.05)	4
97/01/30	50478.80	-	19.33 (.11)	18.55 (.08)	17.76 (.09)	17.41 (.05)	5
97/02/12	50491.50	18.64 (.20)	19.40 (.20)	18.74 (.20)	17.96 (.10)	17.65 (.05)	4
97/03/31	50538.50	-	19.77 (.20)	19.25 (.20)	18.34 (.20)	17.91 (.10)	2

† 1 = Ekar, 2 = Dutch, 3 = ESO 1.5, 4 = MPG-ESO 2.2, 5 = Danish, 6 = IAUC 6379, where instruments are coded as in Tab.1.

Table 7. Main information on the SNe sample.

SNe data	2009dd	2007pk	2010aj	1995ad	1996W
α (J2000.0)	$12^h05^m34^s.10$	$01^h31^m47^s.07$	$12^h40^m15^s.16$	$06^h01^m06^s.21$	$11^h59^m28^s.98$
δ (J2000.0)	+50°32'19".40	+33°36'54".70	-09°18'14".30	-23°40'28".9	-19°15'21".9
parent galaxy	NGC 4088	NGC 579	MGC -01-32-035	NGC 2139	NGC 4027
	SAB(rs)bc	Scd:	SAB(rs)bc	SAB(rs)cd	SB(s)dm
offset from nucleus	1".5 W, 4".0 S	7".4 E, 1".6 S	12".4 W, 11".7 S	25" W, 5" S	17" W, 34" N
12+log(O/H)	8.59	8.50	8.63	8.60	8.60
adopted distance modulus (μ^*)	30.74 ± 0.15	34.23 ± 0.15	34.71 ± 0.15	31.80 ± 0.15	31.93 ± 0.15
SN heliocentric velocity† (km s^{-1})	1025 ± 15	5116 ± 16	6386 ± 20	1674 ± 14	1779 ± 29
adopted reddening E_{tot}(B-V)	0.45	0.11	0.04	0.04	0.23
observed B peak magnitude	15.07 ± 0.06	16.00 ± 0.15	18.20± 0.6	14.77 ± 0.20	15.45 ± 0.03
absolute B peak magnitude	$\leq -17.61 \pm 0.27$	−18.70 ± 0.23	−17.23 ± 0.18	−17.18 ± 0.26	−17.59 ± 0.26
explosion (JD)	2454925.5 ± 5	2454412 ± 5	2454265.5 ± 4	2449981 ± 3	2450180 ± 3
L_{bol} peak (×10^{42} erg s^{-1})	2.16	6.26	2.68	1.55	1.85
light curve peak (JD)	2454937 ± 4	2454420 ± 2	2454269 ± 4	2449989 ± 4	2450186 ± 4
late time decline mag [(100d)$^{-1}$]	1.07	unknown	4.06	0.88	0.86
M(^{56}Ni)	0.029 M$_\odot$	unknown	<0.007 M$_\odot$	0.028 M$_\odot$	0.14 M$_\odot$
M(ejecta)	8.0 M$_\odot$	unknown	9.5 M$_\odot$	5.0 M$_\odot$	unknown
explosion energy (×10^{51} erg)	0.2	unknown	0.5	0.2	unknown
interaction evidences	X, HVHα	X, blue continuum, narrow CS Hα	none	flat-topped Hα, possible HVHα and HVHβ	HVHα, HVHβ
mass loss (M$_\odot$ yr^{-1})	$\gtrsim 10^{-6}$	$\gtrsim 10^{-5}$	–	$\sim 10^{-6}$	$\sim 10^{-6}$

* provided by NED
† corrected for Virgo infall

nitudes. Our estimates of the ultraviolet photometry is in agreement with those presented by Pritchard et al. (2012) as the optical before the transformation into the Johnson–Cousins system.

The light curves are plotted in Fig. 7. The very early observations show a rise to maximum (on JD 2454417.5±1.0 in the B band). The somewhat slower rise in the R band might be an effect of the large errors affecting the measurements of Nov. 12, 2007. Afterward the light curves resemble those of normal SNe II, flatter with a more pronounced plateau at longer wavelengths than at the shorter ones. The rise to the B-band maximum (∼5d)

is also consistent with the phases derived from the spectral comparison performed with "GELATO" (Harutyunyan et al. 2008). Therefore, hereafter we will adopt JD 2454412±5 (November 7.5 UT) as an estimate for the explosion epoch.

Having established the distance and the extinction for this object in Sect. 2, we can determine the absolute magnitudes at maximum: $M_B^{max} = -18.70 \pm 0.23$, $M_V^{max} = -18.44 \pm 0.24$, $M_R^{max} = -18.64 \pm 0.25$ and $M_I^{max} = -18.52 \pm 0.26$, where the associated errors include the uncertainty on the adopted distance modulus and measurement errors. Therefore, SN 2007pk is a
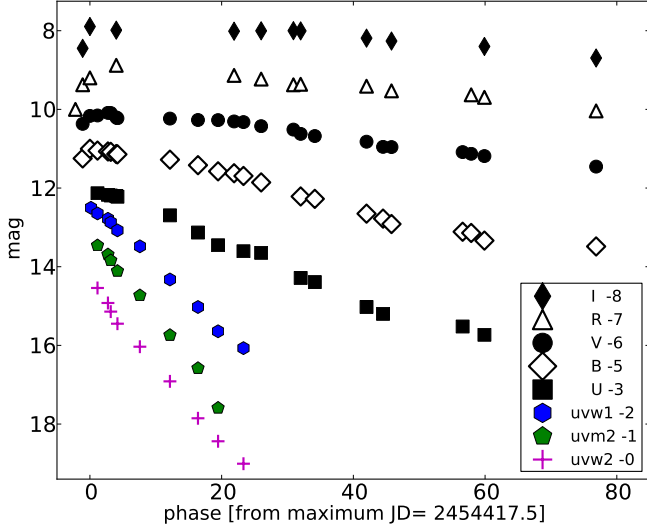
Fig. 7. Synoptic view of the light curves of SN 2007pk in all available bands. The magnitude shifts with respect to the values reported in Tab. 3 are listed in the insert.
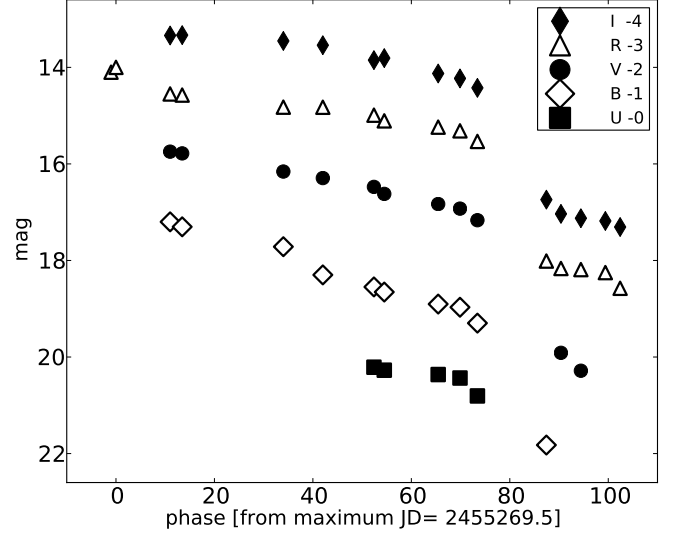

Fig. 8. Light curves of SN 2010aj in optical bands. The magnitude shifts with respect to the values reported in Tab. 4 are in the legend.

bright SN II according to the criteria of Patat et al. (1994); Li et al. (2011). After the peak, the decline of the light curves is similar to those of type IIL SNe, especially in the B band, but with a very slow decline in the red bands. The behaviour of the light curves may resemble that of type IIL SNe such as SN 1979C rather than that of the SNe IIP selected as comparison objects in Sect. 3.4. In fact the average decline rate is $\beta_{100}^B(07pk) \sim 3.7$ mag $(100d)^{-1}$, closer to type IIL SNe than to type IIP SNe Patat et al. (1994), even if the $\beta_{100}^V(07pk) \sim 1.7$ mag $(100d)^{-1}$ typical of type IIP, making SN 2007pk a transitional object between the two subclasses.

3.2.3. SN 2010aj

Our observations (cfr. Tab. 4 and Fig. 8) of the region of SN 2010aj cover a period of almost one year, although the SN has only been detected until ∼100 d after its discovery. Because of the complex background, the late time photometry was performed using the template subtraction. The large errors at late times, estimated with the artificial stars method, are caused by non ideal sky conditions.

The early magnitudes reported in the CBET, give a weak indication that the R band peak occurred around JD 2455269.5 (March 13 UT), in agreement with the spectral age reported by Cenko et al. (2010) and with the epoch provided by the GELATO comparisons. Then we adopted JD 2455265.5±4.0 (March 10 UT) as epoch of the explosion.

The maximum absolute magnitudes are similar to those of the other SNe of our sample: $M_B^{max} \leq -16.95 \pm 0.18$, $M_V^{max} \leq -17.06 \pm 0.17$, $M_R^{max} = -17.80 \pm 0.16$ and $M_I^{max} \leq -17.44 \pm 0.16$, where the reported errors include the uncertainties in our photometry, in the adopted distance modulus, and in the interstellar reddening. Note that only in the R band the reported value is the absolute magnitude at maximum, while in the other bands they are the maxima of our data set. The early post maximum decline is visible only in the R band (∼ 0.55 mag in 11d), since data are missing in other bands.

After about 15 days we observe a long slanted plateau during which magnitudes decline faster at shorter wavelengths. The

plateau is visible in the V, R and I bands with average magnitudes V∼ 18.2, R∼ 17.8 and I∼ 17.5 ($M_V \sim -16.6$, $M_R \sim -17.0$ and $M_I \sim -16.3$), while the B band shows a monotonic decline. The plateau of SN 2010aj is, therefore, relatively luminous when compared with that of more typical SNe IIP and similar to that of SNe 2009bw ($M_V \sim -17.2$, Inserra et al. 2012a) and 2009dd ($M_V \sim -16.8$, cfr. 3.2.1). The tail has been observed in the V, R and I bands, with a single data point in B band. However, because of the short time baseline we can provide only a guess of the decline rates in the R and I bands, $\gamma_R \sim 3.0$ and $\gamma_I \sim 2.1$. These rates suggest the presence of a mechanism covering the main source (decay of ^{56}Co). The stronger gradient in the bluer bands might suggest ongoing dust formation but we do not have any other information to claim such possibility. The drop in magnitude between the photospheric and the nebular phase is $\Delta(R) \sim 2.5$ mag in ∼16d, similar to that of SN 2009bw (∼2.2 mag in ∼13d).

3.2.4. SN 1995ad

Our observations of SN 1995ad started the day after the discovery by Evans et al. (1995, V ∼ 14.25,), about one week after the first (pre-discovery) detection (R ∼ 15.7, Broughton 1998), and span a period of more than 400 days. SN magnitudes are reported in Tab. 5 and shown in Fig. 9. A pre-discovery detection together with spectroscopic constraints allow us to estimate the explosion epoch to about JD 2449981 ± 3 (on September 20).

At maximum, considering the adopted extinction and distance (Sect. 2), this object has $M_B^{max} = -17.18 \pm 0.26$, $M_V^{max} = -17.24 \pm 0.22$, $M_R^{max} = -17.22 \pm 0.22$ and $M_I^{max} = -17.12 \pm 0.15$.

After the peak the light curves show a steep decline from the maximum to the plateau, which then lasts about 50 days (with an average $M_V \sim -16.6$) and resembling that of SN 2007od, SN 1992H and SN 2010aj. Subsequently, starting from about 60 days after the explosion, the luminosity abruptly fades until about 90 days, when the SN reaches the radioactive tail, marked by a decline that is very close to the classical ^{56}Co to ^{56}Fe decay rate ($\gamma_V \sim 0.93$ mag $(100d)^{-1}$ between 95-220d). The available very late time photometry (t>220d) shows an increase of the
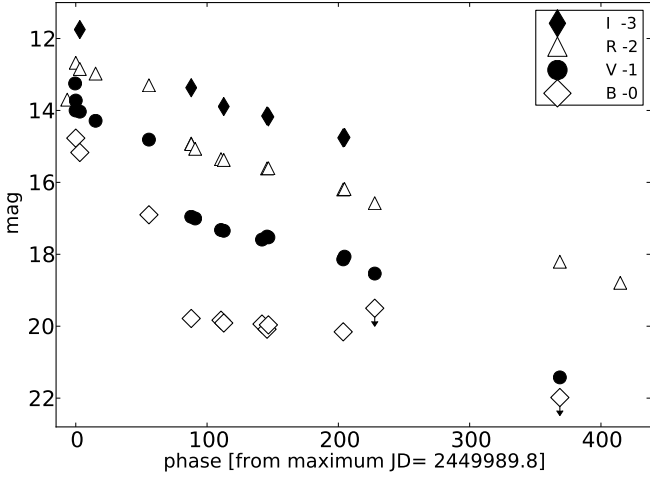
Fig. 9. Light curves of SN 1995ad in uv and optical bands. The magnitude shifts with respect to the original value reported in Tab. 5 are in the insert.
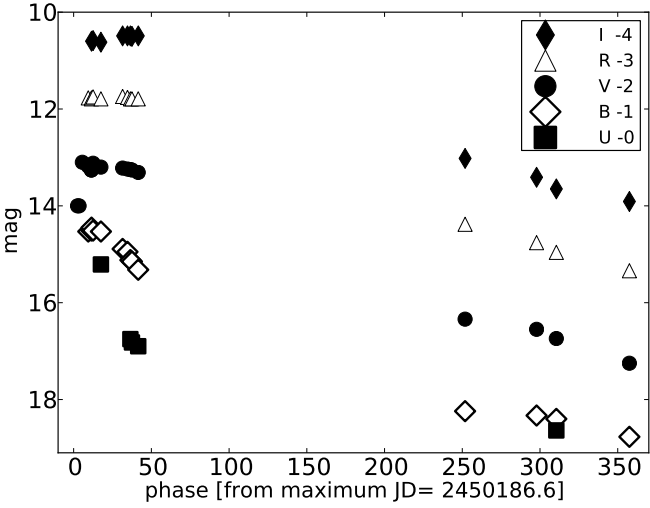

Fig. 10. Light curves of SN 1996W in all available bands. Shifts compared to the original values reported in Tab. 6 are in the legend.

slope in the V and R bands to $\gamma_V \sim 2.02\ \mathrm{mag}\,(100\mathrm{d})^{-1}$ between 21 and 425d. This may be an indication of dust formation, as suggested also by the detection of emission from CO molecules (Spyromilio & Leibundgut 1996).

3.2.5. SN 1996W

Our photometric observations of SN 1996W started a few days after the discovery. The SN magnitudes are reported in Tab 6 along with photometry reported in the IAUC; the light curves are shown in Fig. 10. The early discovery magnitudes and the spectral comparison with the GELATO tool agree in dating the explosion shortly before the discovery. We adopt as epoch of the explosion JD 2450180 ± 3.

Assuming the distance and extinction values discussed in the previous Section, we find $M_B^{max} = -17.59 \pm 0.26$, $M_V^{max} = -17.51 \pm 0.22$, $M_R^{max} = -17.77 \pm 0.20$ and $M_I^{max} \leq -17.78 \pm 0.18$.

The available observations show a flat plateau in the VRI bands during the first ~40 days since explosion with monotonic faster fading in the U and B bands. Then the SN was no longer

Table 8. Main parameters of the SNe II used as reference for our sample.

SN	μ^*	E(B–V)	$M_V^{plateau*}$	Parent Galaxy	References
1979C	31.16	0.01	-	NGC4321	1
1987A	18.49	0.19	-	LMC	2
1992H	32.38	0.03	-17.3	NGC 5377	3
1998S	31.08	0.23	-	NGC 3877	4
1999em	29.47	0.10	-15.6	NGC 1637	5,6
2004et	28.85	0.41	-17.0	NGC 6946	7
2005cs	29.62	0.05	-15.0	M 51	8
2005gl	34.03	0.30	-17.7‡	NGC 266	9
2007od	32.05	0.04	-17.4	UGC 12846	10
2009bw	31.53	0.31	-17.2	UGC 2890	11
2009kf	39.69	0.31	-18.3	SDSS J16	12

* Reported to a $H_0 = 73\ \mathrm{km\,s^{-1}\,Mpc^{-1}}$ distance scale
‡ unfiltered
REFERENCES: 1 - Balinskaia et al. (1980), 2 - Arnett et al. (1989), 3 - Clocchiatti et al. (1996), 4 - Fassia et al. (2001), 5 - Elmhamdi et al. (2003), 6 - Baron et al. (2000), 7 - Maguire et al. (2010), 8 - Pastorello et al. (2009), 9 - Gal-Yam et al. (2007), 10 - Inserra et al. (2011), 11 - Inserra et al. (2012a), 12 - Botticella et al. (2010).
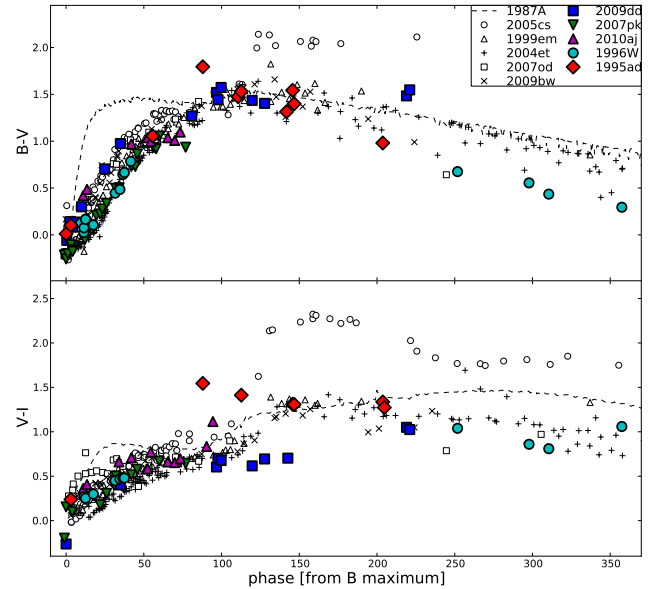

Fig. 11. Comparison of the dereddened colours of our sample of SNe and those of SNe 1987A, 2005cs, 1999em, 2004et, 2007od and 2009bw. The phase of SN 1987A is with respect to the explosion date.

observable. The V band plateau has a bright absolute magnitude of $M_V \sim$-17.5. The SN was recovered at late times, after day 250. The decline rates in the various bands are $\gamma_B \sim 0.50$, $\gamma_V \sim 0.86$, $\gamma_R \sim 0.92$ and $\gamma_I \sim 0.86$ not dissimilar from those expected when the ^{56}Co to ^{56}Fe decay powers the light curve, an exception is the B band, which is flatter.

3.3. Colour evolution

The colour evolution of the five SNe of our sample is valuable to test their degree of homogeneity. These curves are compared in Fig. 11 with those of SN 1987A, the faint SN 2005cs, the normal SN 1999em and the luminous SNe 2004et, 2007od and 2009bw

(Tab. 8). All these SNe IIP show quite similar colour evolution with a rapid increase of the B–V colour as the SN envelope expands and cools down. After about 40 days the colour varies more slowly as the cooling rate decreases, reaching a value of ~1.5 mag at ~100d. The remarkable exceptions to this uniform trend are SN 1987A at early times and SN 2005cs whith a red spike at about 120d, which is a rather common feature in low-luminosity SNe IIP (Pastorello et al. 2004). After 150 days all SNe show a slow turn to bluer colours. Among the new SNe presented in this paper, the B–V colour curve of SN 2009dd seems to be redder although this might be related to an underestimate of the colour excess.

The V–I colour increases for all SNe IIP during the first days past explosion, remains roughly constant during the plateau phase ($V - I \sim 0.7$) and has a further increase during the post-plateau magnitude drop. Then it is fairly constant also during the nebular phase (Fig. 11). The objects of our sample have similar colours as other type IIP SNe at all epochs.

3.4. Bolometric light curve and Ni mass

Unfortunately, because of the lack of simultaneous optical–NIR observations, it is impossible to obtain a true bolometric light curve, so we computed the quasi-bolometric light curves by integrating the fluxes of the available UBVRI photometry (B to I for SN 1995ad). Hereafter we refer to these as bolometric light curves. Broad band magnitudes were converted into fluxes at the effective wavelengths, then were corrected for the adopted extinctions (cfr. Sect. 2), and finally the resulting Spectral Energy Distribution (SED) was integrated over wavelengths, assuming zero flux at the integration limits. Fluxes were then converted to luminosites by using the distances adopted in Sect. 2. The emitted fluxes were computed at phases in which R or V observations were available. When observations in other band were unavailable in a given night, the magnitudes were obtained by interpolating the light curves using low-order polynomials, or were extrapolated using constant colours. The pre-maximum estimates are based mainly on single R- or V-band observations and should be regarded as uncertain.

The bolometric light curves of our sample are displayed in Fig. 12 along with those of the reference SNe of Tab. 8, all distances have been reported to H_0=73 km s^{-1}Mpc^{-1} distance scale. The bolometric peaks of SN 2007pk, SN 2010aj and SN 1995ad are reached close to the R maximum and those of SN 2009dd and SN 1996W closer to the V maximum. The bolometric luminosities at maximum light are reported in Tab. 7. Values range between 1.5 and 6.3×10^{42} erg s^{-1}. The peak luminosities for all objects are moderately bright, only slightly fainter than those of the luminous SNe 2007od, 2004et, 1992H. All the luminosities are significantly lower than the brightest IIP known (SN 2009kf, Botticella et al. 2010) suggesting different explosion mechanism and progenitor from this energetic event. In our sample only SN 2007pk shows a linear decline during the photospheric phase with a rate smaller than that of the prototypical type IIL SN 1979C and a peak luminosity higher than those of all other objects of our sample.

The comparison in Fig. 12 points out the early transition (~80d–100d) to the nebular phase of SN 2010aj, SN 2009dd and SN 1995ad, all with a plateau luminosity similar to that of SN 2009bw.

The tails of the bolometric light curves of SN 2009dd, SN 1995ad and SN 1996W have slopes close to that of the decay of ^{56}Co to ^{56}Fe (cfr. Tab. 7) thus allowing the determination of the ^{56}Ni mass. On the contrary, the observations of SN 2010aj

and SN 2007pk stop before the radioactive tail starts, and no reliable determination on the ^{56}Ni mass is possible.

The ejected ^{56}Ni mass has been derived by comparing the late bolometric light curves integrated over the same wavelength range as SN 1987A, assuming a similar γ-ray deposition fraction

$$M(^{56}Ni)_{SN} = M(^{56}Ni)_{87A} \times \frac{L_{SN}}{L_{87A}} M_\odot \qquad (1)$$

where $M(^{56}Ni)_{87A} = 0.075 \pm 0.005$ M$_\odot$ is the mass of ^{56}Ni ejected by SN 1987A (Arnett 1996), and L_{87A} is the bolometric luminosity at comparable epoch. The comparisons give $M(^{56}Ni)_{09dd} \sim 0.029$ M$_\odot$, $M(^{56}Ni)_{95ad} \sim 0.028$ M$_\odot$ and $M(^{56}Ni)_{96W} \sim 0.14$ M$_\odot$. Making the reasonable assumption that γ-rays from ^{56}Co decay are fully thermalized at late epoch, we cross-checked these results with the formula

$$M(^{56}Ni)_{SN} = \left(7.866 \times 10^{-44}\right) L_t exp \left[\frac{(t-t_0)/(1+z)-6.1}{111.26}\right] M_\odot \qquad (2)$$

from Hamuy (2003), where t_o is the explosion epoch, 6.1d is the half-life of ^{56}Ni and 111.26d is the e-folding time of the ^{56}Co decay, which releases 1.71 MeV and 3.57 MeV respectively as γ-rays (Cappellaro et al. 1997; Woosley et al. 1989). This method provides $M(^{56}Ni)_{09dd} \sim 0.027$ M$_\odot$, $M(^{56}Ni)_{95ad} \sim 0.025$ M$_\odot$ and $M(^{56}Ni)_{96W} \sim 0.13$ M$_\odot$, in agreement with previous determination. We also estimated for SN 2010aj an upper limit $M(^{56}Ni)_{10aj}< 0.007$ M$_\odot$, based on the last epoch in which the SN was detected. We should note that in general we expect a little contribution of the NIR bands at the nebular phase (~15%–20% of the total flux; cfr Inserra et al. 2011).

From the analysis presented here the bright photospheric light curves appear to be the only observable property in common for the objects of our sample.

4. Spectroscopy

The five SNe presented in Section 3 have been observed also in spectroscopy, and well covered until the nebular phase (cfr. Tab. A.6). In this Section we present and discuss our spectra.

All spectra were reduced (including trimming, overscan, bias correction and flat-fielding) using standard routines of IRAF. Optimal extraction of the spectra was adopted to improve the signal-to-noise (S/N) ratio. Wavelength calibration was performed using spectra of comparison lamps acquired with the same configurations as the SN observations. Atmospheric extinction correction was based on tabulated extinction coefficients for each telescope site. Flux calibration was done using spectro-photometric standard stars observed in the same nights with the same set-up as the SNe. Absolute flux calibration was checked by comparison with the photometry, integrating the spectral flux transmitted by standard *BVRI* filters and adjusted by a multiplicative factor when necessary. The resulting flux calibration is accurate to within 0.1 mag. The spectral resolutions in Tab. A.6 were estimated from the full widths at half maximum (FWHM) of the night sky lines. When possible we used the spectra of standard stars to remove telluric features in the SN spectra.

4.1. Individual properties

1. SN 2009dd. Six spectra are available for this object. Fig. 13 shows the entire evolution from about 10d post explosion to about fourteen months. The first spectrum shows a blue continuum comparable to that of other young SNe II. It is characterised by P-Cygni features of the H Balmer series, He I λ5876, Fe II multiplets (e.g. $\lambda\lambda$4924, 5018, 5169) and
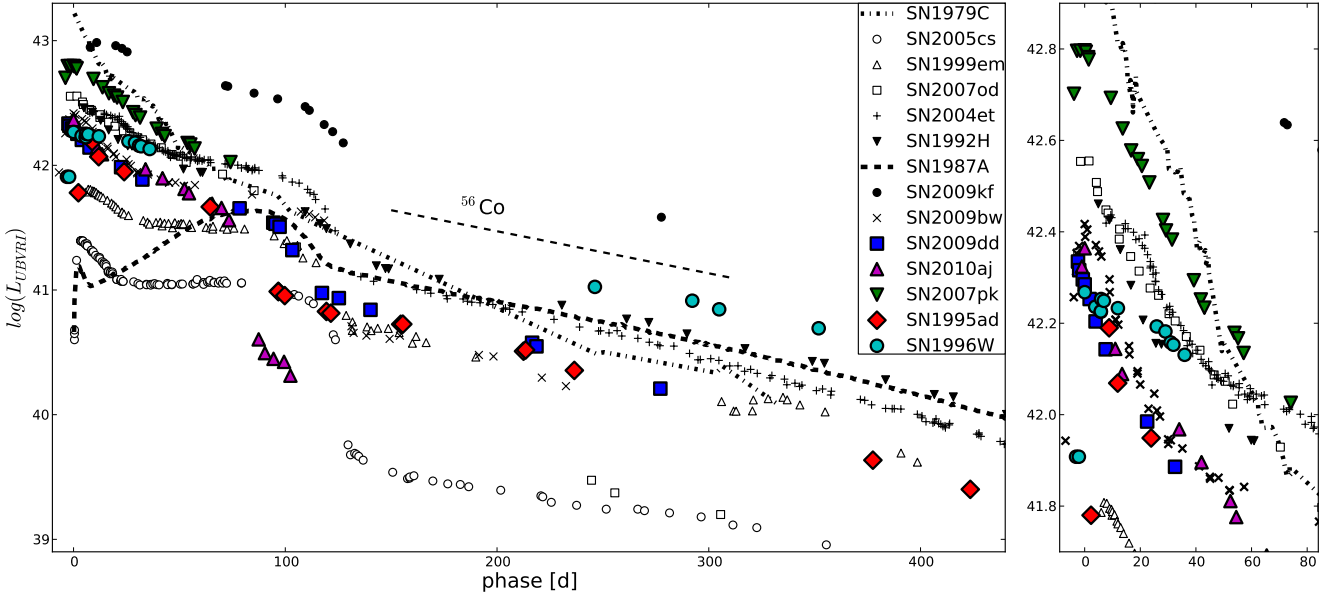
Fig. 12. Comparison of quasi-bolometric light curves of our sample (UBVRI-integrated for SN 2009dd, SN 2007pk, SN 2010aj and SN 1996W and BVRI-integrated for SN 1995ad) with those of other type II SNe. The phase is with respect to the maximum, only for SN 1987A is with respect to the explosion epoch. Minor misalignments in the epoch of maxima are due to the different epochs adopted for the maxima of the reference band light curve and the quasi-bolometric curve. On the right a blow up of the SNe of our sample in the first 80d.

Fig. 13. The complete spectral evolution of SN 2009dd. Wavelengths are in the observer's rest-frame. The phase for each spectrum is relative to the adopted explosion date (JD 2454925.5). The $\oplus$ symbols mark the positions of the strongest telluric absorptions. The ordinate refers to the top spectrum; the other spectra are shifted downwards by 4×10^{-15} (second and third) and 1.4×10^{-15} (others) erg s^{-1} cm^{-2} Å^{-1}.

H&K of Ca II. On the blue side of Hα/ emission, at about 6200Å, three absorption features are present. The bluest, at ~6174Å might be identified with Si II with an expansion velocity comparable to those of the other metallic ions. This line was also identified in other type II SNe (e.g. SN 1992H, SN 2007od, SN 2009bw, Inserra et al. 2011, 2012a, and references therein). The central absorption is possibly re-

lated to Fe II λ6456 but the line strength suggests an optical depth uncommon for metal lines at this stage. Similarly also the Fe II multiplet λ5169 presents a deeper absorption. Alternatively this line is maybe associated to an high velocity component (HV) of Hα. Actually a tiny absorption blue ward of Hβ is visible at ~4620Å but the resulting expansion velocity would be larger than the Hα component: HV(Hα)= 13800 km s^{-1} vs. HV(Hβ)= 14800 km s^{-1}. The presence of HV features could be signature of an early interaction with a CSM (Chugai et al. 2007), supported also by X-ray detection (cfr. Sect. 2). Unfortunately, we do not have other spectra at similar epochs to check this issue. The reddest observed component is Hα, providing a photospheric expansion velocity of ~ 11000 km s^{-1}.

The second spectrum is in the plateau phase. It shows well developed P-Cygni profiles of the Balmer series and a number of metal lines as Fe II at ~4500Å and Sc II λ5031 on the red side of Hβ. Fe I and Sc II are visible at about 5500Å, while Na ID has now replaced He I λ5876. Other metal lines clearly visible are Ba II λ6142 and Sc II λ6245. In the red wavelength region (> 7000 Å) the Ca II near-IR triplet ($\lambda\lambda$ 8498, 8542, 8662) is one of the strongest spectral features. In addition, O I at ~7774Å and N II at ~8100Å are possibly detected. The same features are visible in the third (late-photospheric) spectrum (+107d).

The series of nebular spectra (229d-409d) shows emissions of Na ID, [O I] $\lambda\lambda$6300, 6364, Hα, [Fe II] λ7155, [Ca II] $\lambda\lambda$7291, 7324 doublet and the Ca IR triplet. In the latest spectrum (409d) the SN is still visible (through the [O I], [Fe II] and [Ca II] features) though heavily contaminated by the underlying H II region (Hα, [N II], [S II]).

2. SN 2007pk. Fig. 14 shows the entire photospheric evolution of SN 2007pk from few days post explosion (~4d) to about three months, plus two spectra at ten and eleven months,

when the SN was barely visible and narrow lines from the underlying H II region are mostly detected.

The first spectra (4d-8d) show a blue continuum without prominent absorption features. Hα and Hβ have only emission components. As reported in Parisky et al. (2007), there are some features typical of type IIn SNe (narrow emission components and blue continuum). The prominent feature on the Hβ blue side is identified as He II λ4686 possibly contaminated by CIII/NIII as in the case of SN 1998S (Fassia et al. 2001). Broad Balmer line absorptions appear on day 8 (although they are still weak). This suggests that SN 2007pk is an interacting core-collapse SN.

The spectrum at 27d shows well-developed P-Cygni profiles of metal elements such as Fe II at $\sim$4500Å and Sc II λ5031. Also the Fe II multiplet $\lambda\lambda$4924, 5018, 5169 and Sc II λ6245 are visible. The Na ID feature is blended with He I λ5876. The Hα and Hβ still show a prominent emission with an absorption component comparable with those of other SN II at the same phase. Nevertheless, their profiles display also flat, blue shoulders, possibly a further evidence of a residual interaction of the SN ejecta with the CSM. The 27d spectrum gives a rare snapshot of the spectral evolution from a type IIn to a mildly interacting type II SN.

The last set of photospheric spectra (50d-81d) show the evolution of a more canonical type II during the H recombination phase. Fe I λ4541, Sc II λ5527, Ba II λ6142, Na ID, O I λ7774 are visible as well as the Ca II near-IR triplet ($\lambda\lambda$8498, 8542, 8662).

P-Cygni line profiles of Paschen series, in particular Paβ, Paγ and Paδ are visible in the day 66 NIR spectrum (Fig. 15). Paγ is blended with He I λ10830.

The two late-time spectra (phases 302d to 330d) do not show unequivocal SN features. The narrow unresolved emissions are probably related to the underlying H II region, i.e. Hα ($\Delta v\sim$800 km s^{-1}), [NII] λ6583 and the [S II] $\lambda\lambda$6717, 6731 doublet.

3. SN 2010aj. Its evolution is shown in Fig. 16. It spans $\sim$2 months during the photospheric phase, complemented by an additional observation in the nebular phase, about one year after the explosion.

The first spectrum shows weak absorption profiles of the Balmer lines, He I λ5876, Ca II H&K, Fe II lines ($\lambda\lambda$4924, 5018, 5169), and possibly Si II λ6355, O I λ7774 and the Ca II IR triplet. In the following three spectra (38d - 73d) other metal lines become prominent, including Ti II blends around 4100Å, while Fe II and Ba II contribute to the feature at $\sim$4930Å. Fe I and Sc II lines are also clearly detected at about 5500Å, as well as Sc II λ6245. In these spectra a Na ID feature replaces He I λ5876. The H Balmer lines develop well-designed P-Cygni profiles, always contaminated by the strong narrow components due to an underlying H II region. We can not perform a more detailed analysis as in the other SNe of the sample because of sparse temporal sampling.

The late-time spectrum does not show any sign of broad lines due to the SN. The Hα, Hβ, [O III] and [S II] resolved lines are related to the host galaxy H II region. Because of the modest resolution ($\Delta\lambda = 17$Å) of the last spectrum, we can not exclude that Hα is blended with [N II]. Also the blue continuum is probably due to the contamination from a nearby cluster of young hot stars.

4. SN 1995ad. The available spectra cover a period from one weak until over 500 days after the explosion (see Fig. 17). The spectral evolution is quite representative for a type IIP

SN. The continuum is very blue at the first epoch and progressively turns to a redder colour. The features that are visible are those usually detected in type II SNe during the photospheric phase (e.g. H Balmer series, He I/Na ID, Fe II, Ca II, Sc II and other metal lines). Also the line profiles evolve in a rather standard fashion, from broad P-Cygni profiles (with a weak Hα absorption) at the early epoch to narrow emissions during the nebular phase. The Hα profile in the early phase (9d-24d) reminds that of SN 2007od at a similar stage. The emission in the first two spectra seems somewhat flat-topped and the profile barely shows an absorption component. Only starting from the third spectrum the absorption component becomes significant. It is possible that the flat profile is the result of blending of blueshifted SN emission with the narrow H II region emission. However, as suggested by the extensive analysis of SN 2007od spectra (Inserra et al. 2012b), it could also be caused by the interaction between the ejecta and the CSM ejected by the progenitor soon before exploding as a SN.

The two spectra of the mid photospheric period (60-61d) show the possible contribution of Ti II lines in the bluer part of the spectra (<4500 Å). Also prominent are the lines of Ba II, Fe II and Sc II in the zone around 5000 Å, the strong Sc II λ5527 as well as the lines belonging to Ba II at 5475 Å and 6085 Å whose strengths resemble those in SN 2009bw. Besides the evident Ca II NIR triplet, in the red side of the spectra we identify lines of O I λ7774, N I at 8120 Å and the O I λ9260. By comparison with SN 2009bw the absorption feature at 9030 Å is maybe C I. The presence of the oxygen lines becomes more clear in the spectra of the pseudo-nebular phase (97-99d).
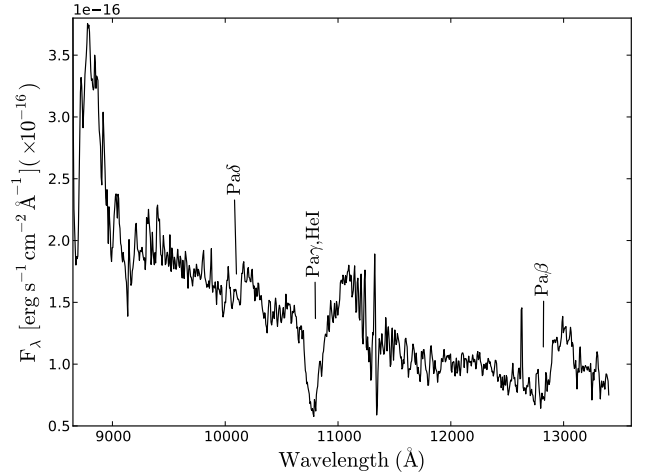

Fig. 15. The NIR spectrum of SN 2007pk at $\sim$ 66d after the explosion date (JD 2454412). Wavelengths are in the observer's rest-frame.

As additional evidence of the early interaction we note that, in analogy with what was observed in photospheric spectra of SN 1999em and SN 2004dj (Chugai et al. 2007), HV Hα and HV Hβ features are possibly detected in our plateau phase spectra (60d and 61d) at a velocity of $\sim$10500 km s^{-1}, which is $\sim$3000 km s^{-1} faster than the photospheric velocities of Hα and Hβ. However, we note that the identification
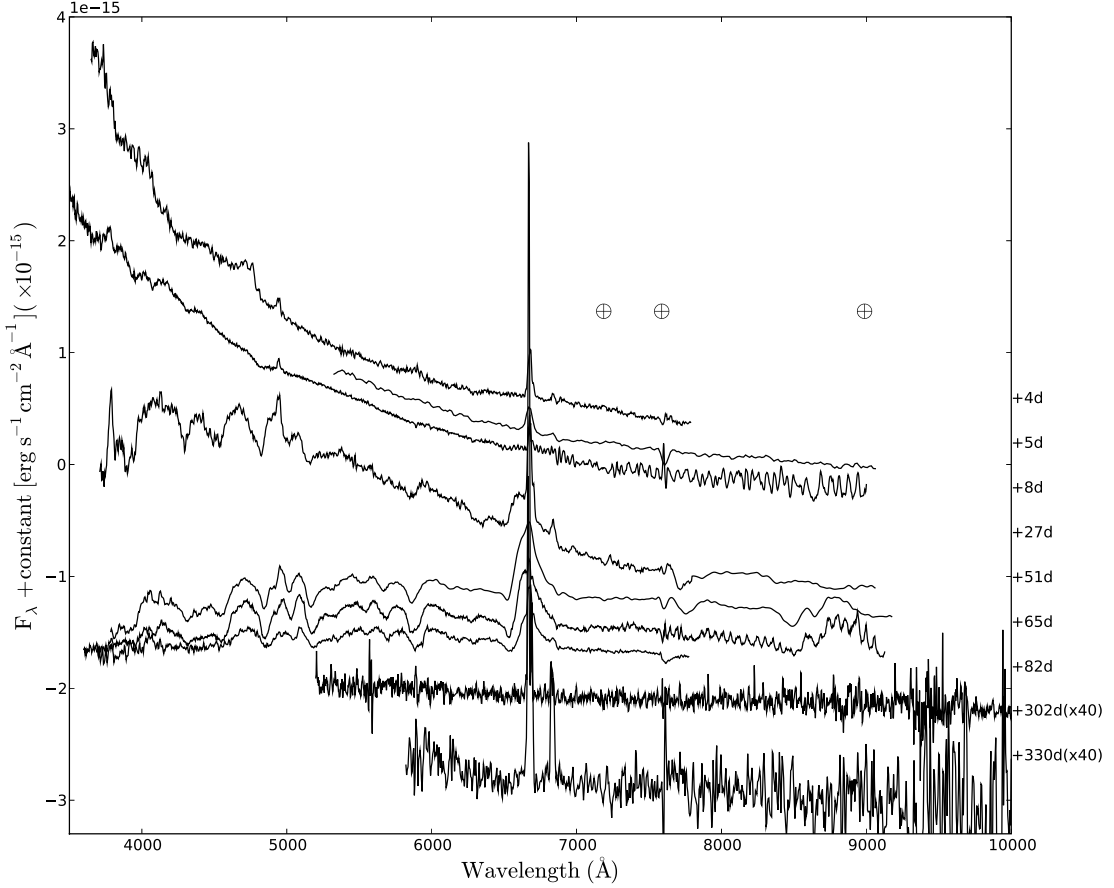
Fig. 14. The spectral evolution of SN 2007pk. Wavelengths are in the observer's rest frame. The phase reported for each spectrum is relative to the explosion date (JD 2454412). The ⊕ symbols mark the positions of the strongest telluric absorptions. The ordinate refers to the top spectrum; the other spectra are shifted downwards with respect to the previous one by 7×10^{-16}, except the third, which is shifted by 1×10^{-15} erg s^{-1} cm^{-2} Å^{-1}

of these HV features is not as firm as in the case of SNe 1999em, 2004dj and 2009bw.

We finally note that [O I] and [Ca II] lines are clearly visible in the nebular spectra. In the last spectra (151–506d) the [S II] $\lambda\lambda 6717$, 6731 of the underlying H II region.

5. SN 1996W. The observations of SN 1996W (cfr. Fig. 18) cover the first couple of months after the explosion, then the object went behind the sun. Later on, the object was recovered during the nebular phase (252 − 312 days), when 3 high-S/N spectra were obtained.

The evolution of this SN matches very well that of normal type IIP SNe, although the line velocities and the continuum temperatures are somewhat higher than in canonical SNe IIP at a comparable phase (see Table 7 and Section 4.2). Hα, Hβ and He I are visible in the early spectra, while metal lines are detected after 19d.

In the spectra from 19d to 67d there are the classical Fe II lines between 5000 and 5200 Å as well as other metal lines such Sc II $\lambda 5527$ and the Sc II $\lambda 6246$ although weaker than in SN 1995ad. The same is true for Ba II 5450 Å and 6060 Å that become clearly visible only in the spectrum of 67d, then later with respect to the previous SNe. Also in this SN the spectrum of 67d shows O I $\lambda 7774$, N I at 8110 Å and O I $\lambda 9260$.

Forbidden emissions of the [Ca II] $\lambda\lambda 7291$-7324 doublet, [O I] $\lambda\lambda 6300$-6364 doublet and [Fe II] in the region of 7000–

8200 Å are observed in the nebular spectra as the [S II] doublet of the HII region, but the Na ID and near-IR Ca II features are clearly detected until ~10 months after the explosion.

In summary, the spectroscopic evolution of the objects seems to introduce additional inhomogeneity in the luminous type II SN sample. In fact, four out of five objects show possible evidences of interaction, while the SN 2007pk has a photospheric spectroscopic evolution different from the rest of the sample.

4.2. Velocity and temperature evolution

The expansion velocities provide key information on the energetics of the explosion. In Fig. 19 we show the time evolution of the expansion velocities for our SNe sample as inferred from the position of the minima of the P-Cygni profiles for some representative lines (Hα, Hβ, He I λ 5876, Fe II $\lambda 5169$ and Sc II $\lambda 6246$). The measured expansion velocities are listed in Tab. 9. In all cases the velocities of Hα are systematically higher than those of Hβ. At very early epochs the Hα velocities are close to 12000 km s^{-1} in SNe 1995ad, 1996W and 2009dd, and decline very fast.

The determination of the expansion velocity is problematic in SN 2007pk because of the lack of absorptions possibly due to ejecta-CSM interaction (cfr. Sect. 4.1). The early velocity of
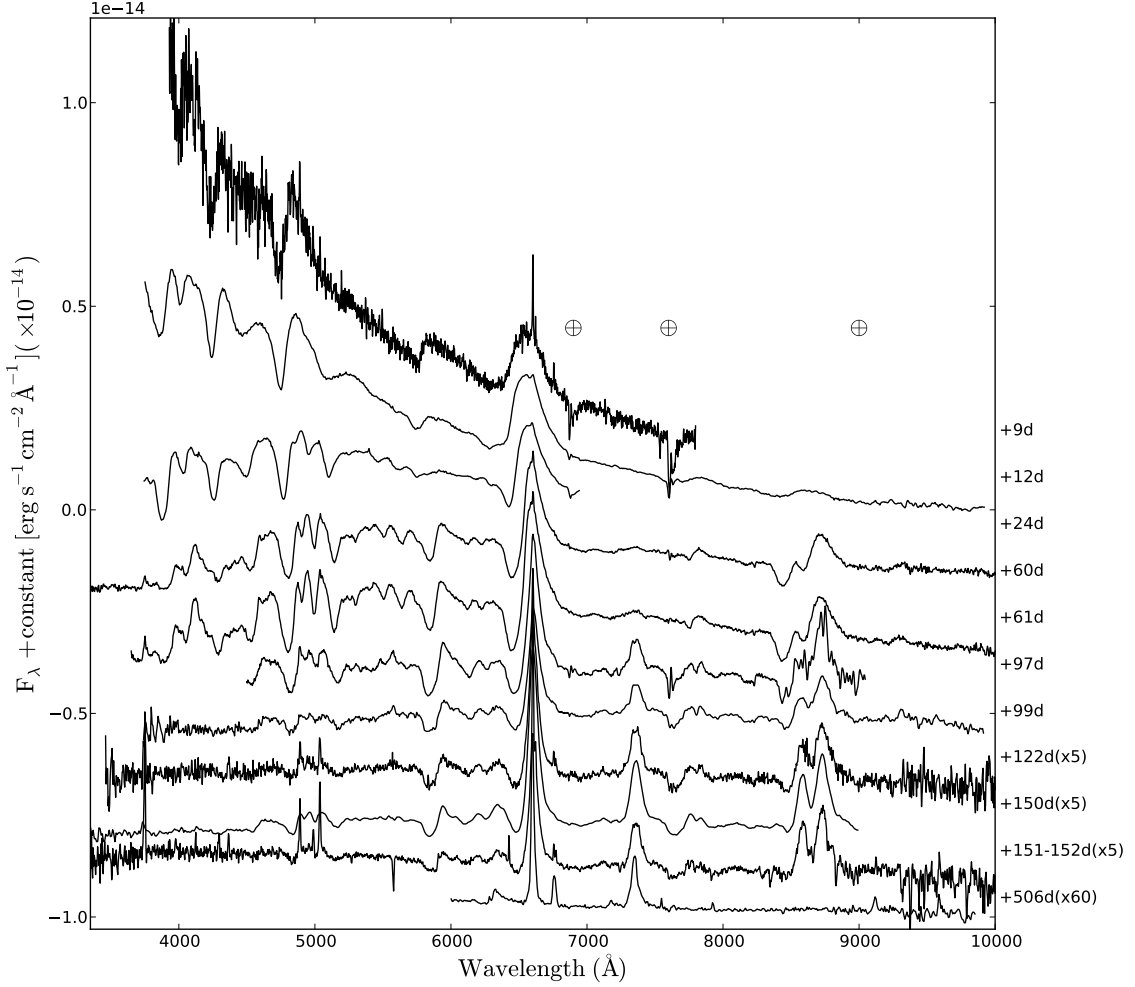
15

Fig. 17. Spectral evolution of SN 1995ad. Wavelengths are in the observer's rest frame. The phase reported for each spectrum is relative to the explosion date (JD 2449981). The ⊕ symbol marks the positions of the most significant telluric absorptions. The second and third spectra are shifted upwards by 1×10^{-15}; the other ones are shifted downwards with respect to the previous by 0.7×10^{-15} erg s^{-1} cm^{-2} Å^{-1}.

the Balmer lines reported in Fig. 19 is the FWHM of the narrow emissions visible up to day +8.

For the epochs in which the He I line is visible, its velocity is significantly smaller than that of Hα. FeII and ScII are good indicators of the photospheric velocity and their values are the smallest among those of the measured lines. Sc II remains always slower than Fe II, having average velocities, for the SNe of the sample, that are the ~90% of those of Fe II.

SN 1996W has metal line velocities that are a factor 1.5 higher than other events whilst the velocities deduced from the H and He I lines are not remarkably different. The higher velocities suggest higher explosion energies, and a different progenitor with respect to the other SNe. The high velocity of the photosphere is at odd with the normal velocities of the outer ejecta. The presence of a weak interaction with a CSM could explain this behaviour (for details see Inserra et al. 2012b), supported by the presence of HV Hα at 11500 km s^{-1} during the entire photospheric evolution (see Sect. 5).

In Fig. 20 we show the comparison of the Hα velocity evolution of our SN sample with that of other classical SNe II. All SNe show a quite similar evolution, also taking into account the uncertainties in the determination of the dates of explosions.

Some degree of individuality is probably present, but all objects appear to be confined in a narrow strip of ± 1000 km s^{-1} during the mid-late photospheric phase, with the exception of the low-luminosity SN 2005cs. The objects of our sample (especially SNe 2009dd, 1995ad and 1996W) seem similar to the weak interacting SN 2009bw.

The bottom panel of the same figure reports the temperature evolution of our SNe and those of the reference sample, derived from the black-body fit of the spectral continuum (see Tab. 9). As suggested before the objects showing some evidence of interaction have higher temperatures during the first 20d than the other SNe II. The temperatures of SN 2009dd and SN 1995ad are the highest of the sample. After 40d the temperatures become quite homogenous lying at T~5500 K.

4.3. Shared interaction signatures

In this Section we highlight possible spectroscopic interaction signatures through a comparison of the early and photospheric spectra with those of other type II SNe. Possible indirect evi-
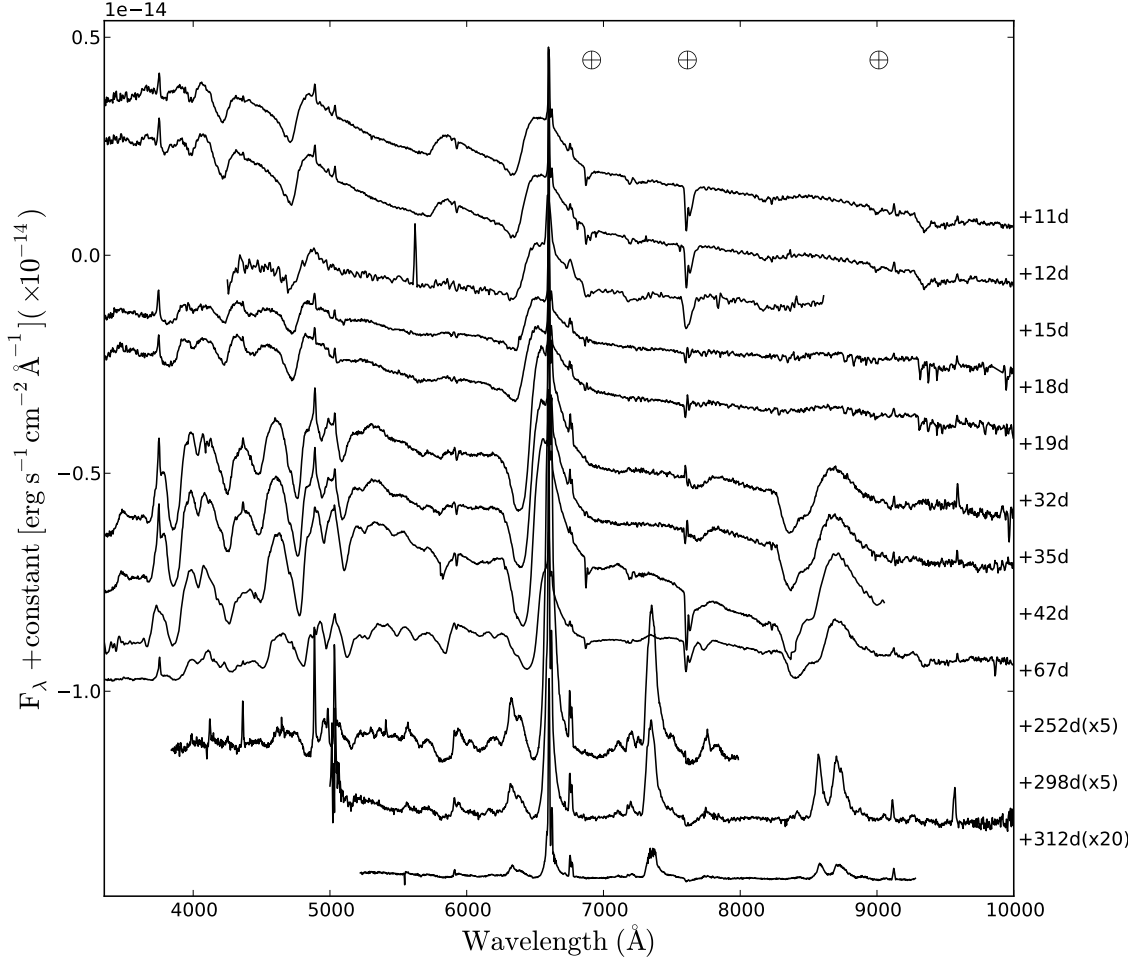
Fig. 18. The overall spectral evolution of SN 1996W. Wavelengths are in the observer's rest frame. The phase reported for each spectrum is relative to the explosion date (JD 2450180). The ⊕ symbol marks the positions of the most important telluric absorptions. The spectra are shifted with respect to the first one.

dences of early, weak[3] interaction are flat topped line profiles as shown by SN 2007od (CSM mass ~ 10^{-4} $M_\odot$, Inserra et al. 2011), and the presence of HV features, originating in the ejecta just below the shock front.

In panel a) of Fig. 21 we compare the early spectra of the type II of our sample with those of other SNe. The boxy Hα profiles previously claimed for SN 1995ad and SN 1996W (Sect. 4.1) appear less consistent compared with that of SN 2007od. In this case the boxy profile is probably due to the contamination of the Hα emission of the H II region on the blueshifted maximum of the SN emission for both the objects. This conclusion is strengthened by the higher velocity and stronger intensity of their Hα absorption lines compared to that of SN 2007od (see Inserra et al. 2012b, for further details about interaction and lower Balmer velocities) as shown in Sect. 4.2. The SN 2009dd Hα emission profile is similar to those of SN 1999em and SN 2009bw without flat component. In Sect. 4.1 we have mentioned three unusual absorptions on the blue side of Hα in SN 2009dd that, to our knowledge, have not been seen before in type II SNe. The bluest component was identified with Si II $\lambda6355$ as in SN 2007od (Inserra et al. 2011, 2012b) and SN 2009bw (Inserra et al. 2012a). The central component might

be a HV feature of Hα with $v = 13800$ km s^{-1} or alternatively Fe II $\lambda6456$ with an unusually large optical depth compared to other Fe II lines of the objects and of the other SNe of the comparison. Although there is no other spectral evidence such as a clear presence of HV Hβ or a flat topped Hα profile, the unusual multiple component absorptions in the Hα profile and the X-ray detection at early times both point to interaction between ejecta and CSM. For the other two objects we note a weak feature on the blue side of the Hα absorption in SN 1996W that could be related to an HV Hα at ~11500 km s^{-1}. For SN 1995ad there is a possible HV Hα at 6280Å with $v \sim 13000$ km s^{-1}. It is barely visible in the 24d spectrum and disappears thereafter.

In the following panel (b) we show the comparison as in the same objects of the previous panel during the plateau phase. At this stage SN 2009bw and SN 1999em already show an HV Hα at ~7300 km s^{-1} (Inserra et al. 2012a) and ~8200 km s^{-1} (Chugai et al. 2007) respectively. The notches of the HV Hα present in the spectra of our sample appear clear in comparison with other interacting objects. HV Hα lines are identified with velocity of: ~13800 km s^{-1} for SN 2009dd, ~11500 km s^{-1} for SN 1996W, ~10500 km s^{-1} for SN 1995ad. The velocities of the HV lines of SN 2009dd and SN 1996W are the same as measured during the early phase (comparison panel a), suggesting that interaction persists during the entire photospheric phase at least for these two objects.

---

[3] We define as weak interaction a phenomenon that does not alter significantly the light curve and the spectral evolution.
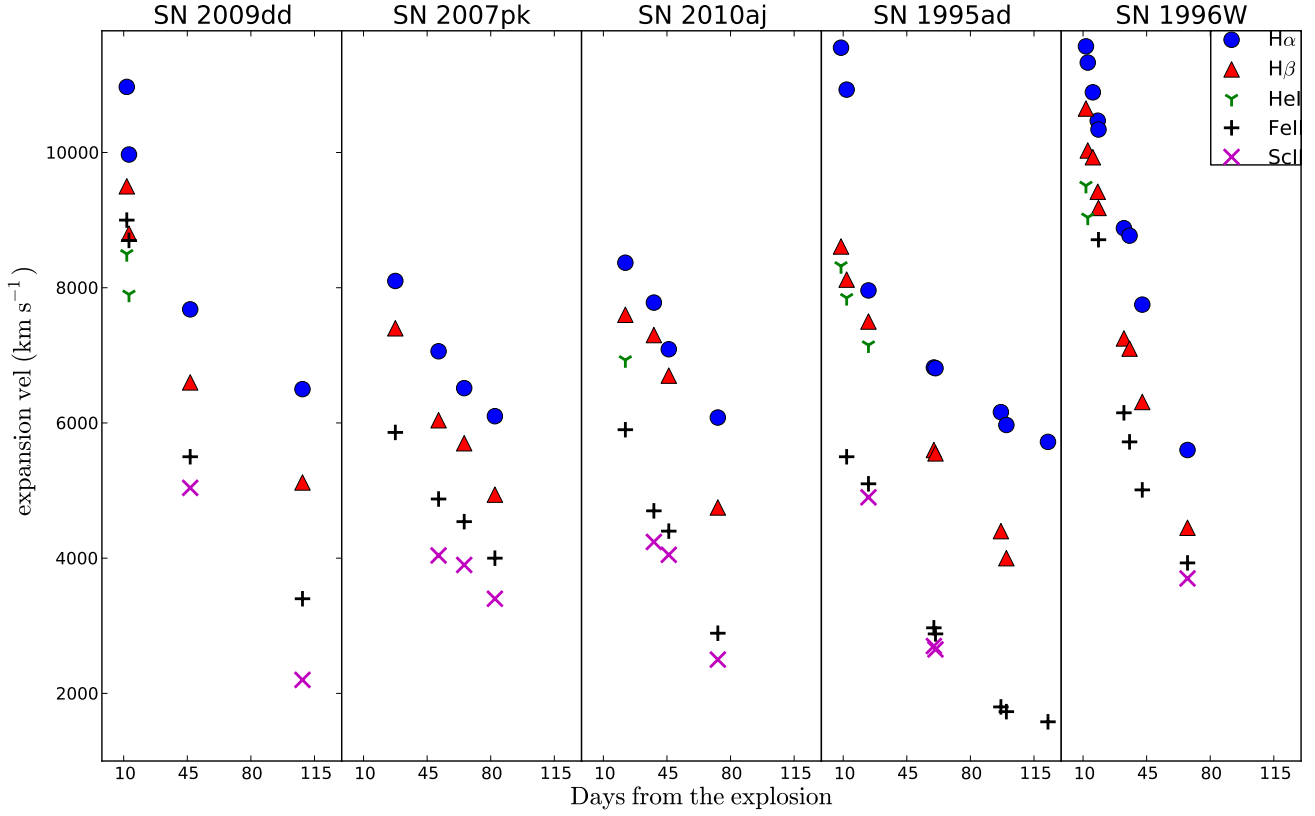
17

Fig. 19. Expansion velocities measured for the SNe of our sample, derived from the position of the P-Cygni minima for the following lines: Hα, Hβ, He I λ5876, Fe II λ5169 and Sc II λ6246. The velocities of the Balmer lines of SN 2007pk up to day +8 given by the FWHM of the narrow emissions are not shown.
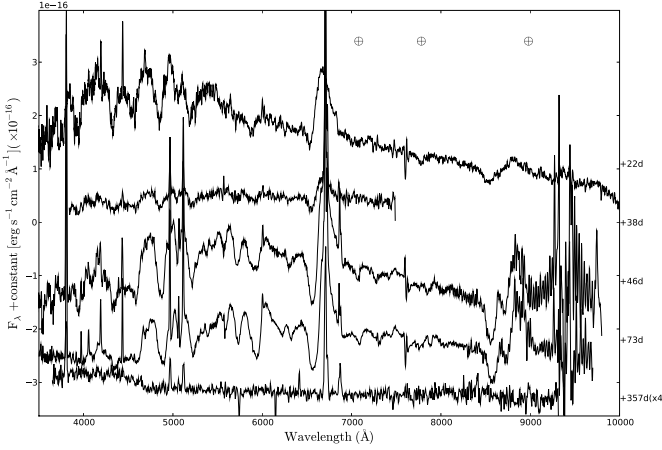

Fig. 16. The spectral evolution of SN 2010aj. Wavelengths are in the observer's rest frame. The phases reported to the right are relative to the explosion epoch (JD 2455265.5). The ⊕ symbols mark the positions of the strongest telluric absorptions. The ordinate refers to the top spectrum; other spectra are shifted downwards with respect to the previous one by 2×10^{-16} and 6×10^{-16} (only the third) erg s^{-1} cm^{-2} Å^{-1}.

Panels c) and d) we show early and late photospheric spectra of SN 2007pk, the only SN of the sample with clear spectroscopic differences from the other objects. We compare the spectra with those of the type IIn SN 1998S, the weakly interacting

type IIP SN 2007od and the type IIn SN 2005gl which show similarities in the spectroscopic evolution. The narrow H Balmer lines and the double-peaked line at ~4600Å, possibly related to highly ionised elements such as C III/N III or C IV, stand out over a very blue continuum. The similarity between the features of SN 2007pk and SN 1998S in the region of 4600Å is remarkable. Also SN 2007pk and SN 2005gl shared not only a similarly blue continuum (T~14000 K) but also a common Hα profile without absorption component and with a FWHM of ~1800 km s^{-1} and ~1600 km s^{-1} respectively. The SN 2007pk spectrum is quite different from that of SN 2007od.

As mentioned in Sect. 4.1 the spectrum of SN 2007pk evolves rapidly and already on day 50, during the plateau, it resembles closely those of standard type IIPs. In panel (d) we compare late photospheric spectra. Again, the similarity between SN 2007pk and SN 2005gl is remarkable. Both show the above mentioned evolution to a classical type IIP spectrum with a well developed absorption component for all the ions. SN 2007pk and SN 2005gl show also deeper absorption components of the Balmer lines with respect to SN 1998S, while the lines of the ions of the inner ejecta like Fe II and Sc II seem to have the same strength. The absorption component of Hα is significantly weaker than in SN 2007od, possibly tweaked by residual interaction (cf. Inserra et al. 2012b).

Table 9. Observed continuum temperatures and line velocities for the objects of our sample.

JD +2400000	Phase† (days)	T (K)	v(Hα) (km s⁻¹)	v(Hβ) (km s⁻¹)	v(He I) (km s⁻¹)	v(Fe II) (km s⁻¹)	v(Sc II) (km s⁻¹)
			SN 2009dd				
54936.7	11.2	14700 ± 2000	10970 ± 150	9500 ± 370	8500 ± 700	9000 ± 500	
54938.4	12.9	14000 ± 2000	9970 ± 150	8800 ± 400	7900 ± 600	8700 ± 500	
54971.6	46.1	5500 ± 200	7680 ± 250	6600 ± 100		5500 ± 500	5040 ± 100
55033.4	107.9	5300 ± 700	6500 ± 300	5120 ± 230		3400 ± 1000	2200 ± 200
			SN 2007pk				
54416.3	4.3*	14500 ± 2000	1800 ± 200	1800 ± 200			
54417.5	5.5*	13500 ± 1000	2300 ± 100				
54421.4	8.4*	12000 ± 1000	2800 ± 500	2000 ± 200			
54439.5	27.5	8500 ± 300	8100 ± 800	7400 ± 100		5860 ± 250	
54463.3	51.3	5500 ± 500	7060 ± 100	6040 ± 200		4875 ± 400	4040 ± 100
54477.4	65.4	5500 ± 300	6515 ± 180	5700 ± 300		4540 ± 100	3900 ± 180
54494.3	82.3	5600 ± 600	6100 ± 100	4940 ± 500		4000 ± 500	3400 ± 400
			SN 2010aj				
55287.6	22.1	8000 ± 500	8370 ± 200	7600 ± 300	6930 ± 1000	5900 ± 700	
55303.3	37.8	5600 ± 500	7780 ± 700	7300 ± 350		4700 ± 200	4240 ± 500
55311.5	46.0	5800 ± 500	7090 ± 300	6700 ± 300		4400 ± 200	4050 ± 200
55338.5	73.0	5200 ± 400	6080 ± 300	4750 ± 380		2890 ± 250	2500 ± 200
			SN 1995ad				
49989.8	8.8	16000 ± 1500	11500 ± 1100	8610 ± 600	8321 ± 600		
49992.9	11.9	9900 ± 400	10930 ± 580	8120 ± 520	7850 ± 400	5500 ± 1500	
50004.9	23.9	8200 ± 600	7960 ± 270	7500 ± 200	7150 ± 300	5100 ± 350	4900 ± 300
50040.8	59.9	6900 ± 500	6820 ± 200	5600 ± 100		2970 ± 100	2700 ± 100
50041.8	60.8	6900 ± 600	6810 ± 210	5550 ± 100		2880 ± 120	2650 ± 100
50077.8	96.8	5400 ± 600	6160 ± 190	4400 ± 300		1800 ± 200	
50080.8	99.8	5300 ± 900	5970 ± 360	4000 ± 500		1730 ± 400	
50103.7	122.7	5700 ± 400	5720 ± 380			1580 ± 210	
50131.7	150.7	5500 ± 900	5570 ± 220			1280 ± 190	
50132.7	151.7	6700 ± 1500	5470 ± 290			1210 ± 200	
50133.7	152.7	7200 ± 1300	5320 ± 205				
			SN 1996W				
50191.6	11.6	10400 ± 300	11570 ± 500	10650 ± 500	9510 ± 500		
50192.6	12.6	10200 ± 300	11330 ± 500	10030 ± 500	9040 ± 500		
50195.4	15.4	10000 ± 200	10890 ± 500	9930 ± 400			
50198.4	18.1	9600 ± 300	10470 ± 500	9420 ± 400			
50198.6	18.5	9500 ± 300	10340 ± 500	9180 ± 400		8710 ± 400	
50212.5	32.5	6800 ± 300	8880 ± 300	7250 ± 300		6150 ± 300	
50215.6	35.6	6700 ± 300	8770 ± 300	7100 ± 300		5720 ± 300	
50222.6	42.6	6600 ± 300	7750 ± 300	6310 ± 300		5010 ± 300	
50247.5	67.5	6400 ± 500	5600 ± 300	4450 ± 300		3930 ± 250	3700 ± 200
50432.8	252.8		3700 ± 200	2830 ± 200			
50478.5	298.5		3600 ± 200				

† with respect to the explosion epochs (cfr. Tab. 7)
* the velocities are the FWHM of the narrow emissions

5. Discussion

In previous Sections we presented the photometric and spectroscopic data of 5 SNe II and discussed their evolution from the photospheric to the nebular phase.

As seen in the previous Sections our SNe sample show to be relatively bright: their average absolute peak magnitude is $M_V \sim -17.8$ (i.e. $L_{peak} \sim 3 \times 10^{42}$ erg s^{-1}), higher than that of standard SNe II (Patat et al. 1994; Li et al. 2011); a plateau shorter (less than 100d) than those of canonical type IIP events; expansion velocities of the ejected material ranging from ~ 10000 km s⁻¹ at early phases to ~ 4000 km s⁻¹ at the end of the photospheric phase, and temperature on the plateau of $T_{ph} \sim 5000$ K. On the other hand, the luminosity evolution of the sample is quite heterogeneous, with the drop from the photospheric to the nebular phase (when visible) occurring at different times and with a different magnitude drop for the 5 SNe. Also

the inferred ^{56}Ni masses span a range of more than 1 order of magnitudes, 1.4×10^{-1} to $7 \times 10^{-3} M_\odot$ (cfr. Sect. 3.4).

Generally these properties are consistent with progenitor stars having an initial (ZAMS) mass of 8–15 $M_\odot$ (Smartt 2009). This mass range consists of two kinds of stars having a different evolutionary path prior to the core collapse event. The first one is formed by the massive super-asymptotic giant branch (SAGB) stars which, after H-, He-, and C-burning, form a degenerate Neon-Oxygen core (e.g. Pumo 2006, 2007, and references therein), where the physical conditions can be suitable for triggering electron-capture reactions on ^{24}Mg and other nuclei which are present in trace amounts in the core, leading to a so-called electron-capture supernova (EC-SN) event (e.g. Pumo et al. 2009, and references therein). The other kind of progenitors are "standard" massive stars at the lower mass range that can produce iron core collapse SNe (Fe CC-SNe), after having ig-
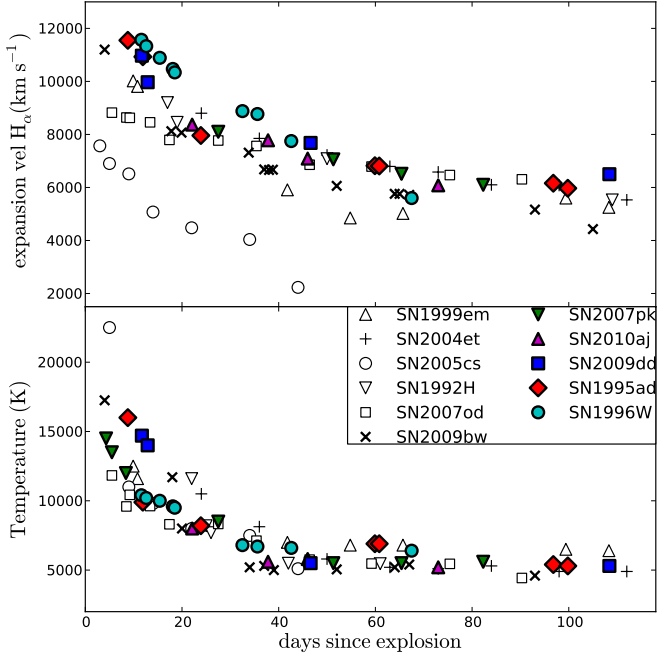
Fig. 20. Top: Comparison of the Hα velocities of our SNe with those of other SNe II. Bottom: Comparison of the continuum temperature evolution of our SNe sample with those of SNe 1999em, 2004et, 2005cs, 1992H, 2007od and 2009bw.

nited all nuclear burnings up to the formation of an iron core (e.g. Woosley & Weaver 1986; Woosley et al. 2002; Heger et al. 2003).

5.1. X-ray and UV signatures

Only two out of five objects had X or UV observations, i.e. SNe 2007pk and 2009dd. The spectral evolution of SN 2007pk shows the rare transition from a type IIn to a non interacting type II SN. To our knowledge the only other object starting as a type IIn and evolving after two months into a standard type IIP is SN 2005gl (Gal-Yam et al. 2007; Gal-Yam & Leonard 2009). Considering also the strong X-ray detection [$L_X(07pk) \sim 1.7 \times 10^{40}$ erg s^{-1} (i.e.10 times larger than those of SN 2009dd and SN 1999em, Immler, Russell, & Brown 2009; Elmhamdi et al. 2003)] we argue that the ejecta-CSM interaction in SN 2007pk was stronger than in SN 2009dd.

The shock emission occurs at soft X-ray or at far-UV wavelengths depending on the SN density profile, with flatter profiles leading to higher shock velocity, higher post-shock temperature and hence higher frequencies emission (Chevalier & Fransson 1994). SN 2009dd and SN 2007pk have been monitored in the Swift UV bands and we can compute the contribution of the UV to the bolometric emission (Fig. 22). Both SNe show higher UV fluxes than SN 2007od suggesting stronger interaction, maybe due to an enhanced mass loss or a different CSM density profile.

SN 2007pk UV flux decreases steeper (Fig. 22) than in the other two SNe with interaction until ~10d from the optical B maximum. The flux of the two early interacting SNe of our sample is higher than the normal IIP SN 2008in (Roy et al. 2011). Later on, the fluxes flatten, suggesting a decrease of the intensity of the interaction (also confirmed by the evolution of the SN 2007pk spectrum 27d after explosion). The analysis of the SN 2007pk flux at wavelengths shorter than optical and its com-

parison with those of weak interacting SNe (e.g. SNe 2007od and 1999em) gives us information about the SN density profile. The SN 2007pk UV flux is twice as high as that of SN 2007od, while the SN 2007pk X-ray flux is 10 times stronger than that of SN 1999em, suggesting a flatter density profile for SN 2007pk than SNe 2007od and 1999em. SN 2009dd seems to have a similar UV evolution as SN 2007od, suggesting a similar density profile and interaction strength for these two SNe.

5.2. HV signatures and mass loss

As reported above the spectroscopic evolution introduces additional diversity. HV components in the Balmer lines, flat-topped Hα profiles and the peculiar early spectroscopic evolution of SN 2007pk suggest the presence of weak to moderate ejecta-CSM interaction. From our investigation, four out of five objects show Balmer lines with structured profiles (HV components, boxy or multicomponent profiles), whilst only SN 2010aj shows a canonical spectrum. Similar signatures have been observed in SNe 1999em, 2004dj (Chugai et al. 2007), 2007od (Inserra et al. 2011) and 2009bw (Inserra et al. 2012a), and in all cases were interpreted as evidence of weak interaction with a nearby CSM.

In the case of SN 1996W there is some evidence of early time interaction of normal SN IIP ejecta with a CSM in analogy to what has been observed in SN 1999em, SN 2004dj, SN 2007odand SN 2009bw (Chugai et al. 2007; Inserra et al. 2011, 2012a). Chugai et al. (2007) have shown that the interaction of the ejecta of a SN IIP with an average RSG wind can be detected during the photospheric phase through the emergence of absorptions (shoulders) on the blue wings of the undisturbed H lines due to enhanced excitation of the outer un-shocked ejecta. In SN 1996W we identify two features on the blue side of Hα and Hβ as HV Hα and HV Hβ, respectively. Differently from SN 1995ad, for SN 1996W these lines are detected starting from the first available spectrum (11d) until the last photospheric spectrum (67d) at a velocity of ~11500 km s^{-1}. We find also a possible second HV feature at ~12500 km s^{-1}, but it is visible only in the Hα region. In Fig. 23 we show the evolution of the HV features compared with the corresponding Balmer lines. The velocity of these two HV features is constant (see Fig. 23). We should note that the position of these lines is compatible with the expected position of Fe II lines at the earliest epochs, but the lack of velocity evolution does not favour this identification.

Following Chugai et al. (2007) we can argue that the HV features in SN 2009dd formed in a cool dense shell (CDS) behind the reverse shock, allowing the formation of a notch, a shallow and narrow absorption, very similar to that shown by SN 2004dj. The presence of HV features at an early phase (<20d) suggests a prolonged interaction compared to in SN 1999em, SN 2004dj and probably SN 2009bw. The low luminosity at X-ray wavelengths does not conflict with this scenario, because the H excitation of the CDS gas is presumably maintained by the absorption of the X-rays emitted from hot material behind the reverse shock, allowing for an intrinsic X-ray production much greater than that observed.

Line profile models of the HV features in SN 2009dd suggest a typical red supergiant with a dimensionless wind density parameter $w = \dot{M}_{-6}/u_{10} \gtrsim 1$ (where $\dot{M}_{-6}$ is the mass loss rate in units of 10^{-6} M$_\odot$ yr^{-1} and u_{10} is the wind velocity in units of 10 km s^{-1}), i.e. $\dot{M} \gtrsim 10^{-6}$ M$_\odot$ yr^{-1}, higher than those of SNe 1999em and 2004dj (Chugai et al. 2007). Assuming a typical wind duration of 10^6 yr, the mass lost by the progenitor star would be slightly higher than 1M$_\odot$. Likewise, we can analyse the HV absorptions of the other SNe. SN 1995ad and SN 1996W
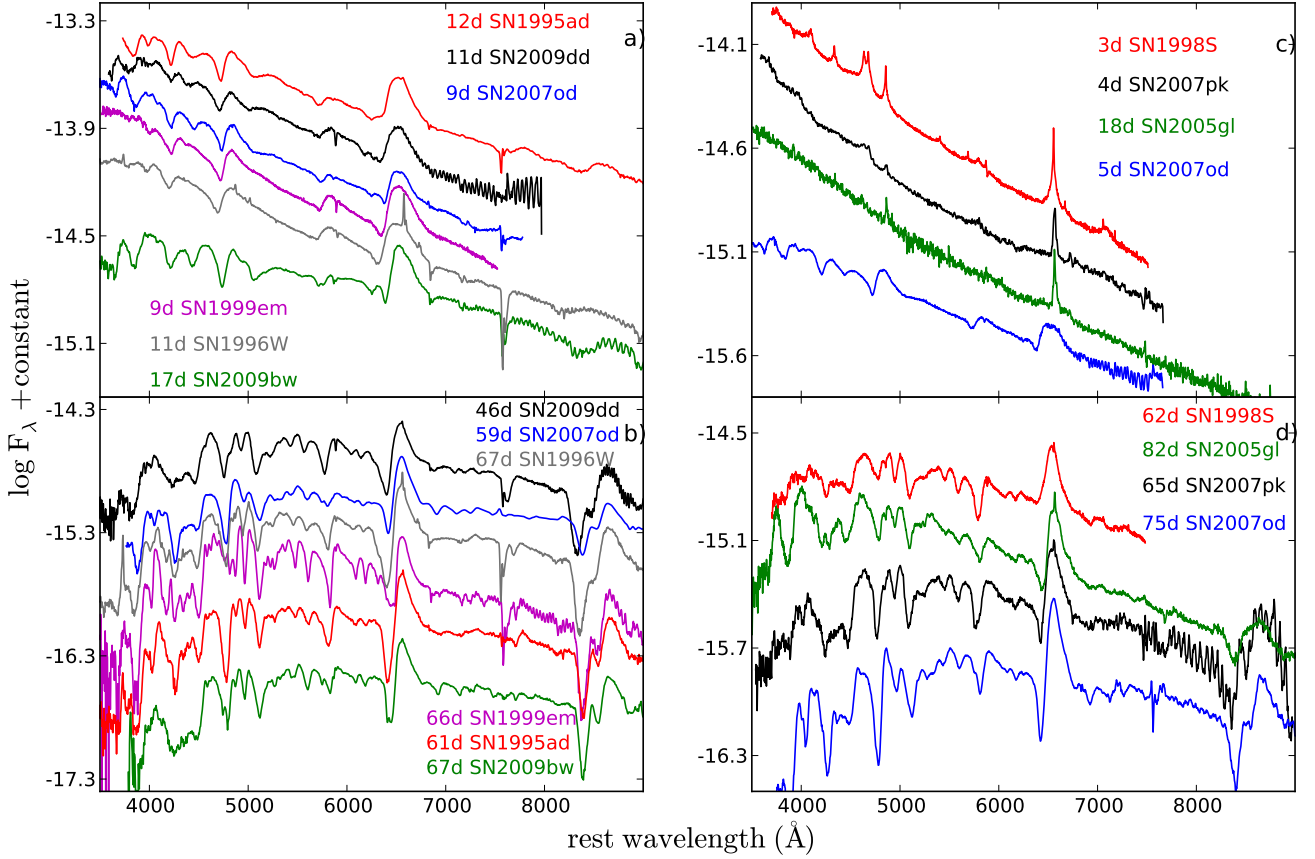
Fig. 21. Panel a): Comparison between some early spectra of our sample and those of the interacting SNe 1999em, 2007od and 2009bw. Panel b): The same objects as in the previous panel compared during the plateau phase. Panel c): Comparison among early spectra of SN 2007pk, with those of other strong (SNe 1998S and 2005gl) and weak (SN 2007od) interacting SNe. Panel d): The same objects compared during the plateau phase. The shock breakout day of SN 2005gl is the middle JD of the window reported in Gal-Yam et al. (2007). For references, see the text and Tab. 8.

show shallower absorptions components, suggesting the formation of the absorption in the shocked ejecta, in the layer excited by X-rays from the reverse shock. Assuming also for these a typical wind of $w \sim 1$, the mass loss from the progenitor star is of the order of $\dot{M} \sim 10^{-6}$ $M_\odot$ yr^{-1} corresponding to a rough value ≤ 1 $M_\odot$ of expelled mass. Using the same arguments presented here, it appears to be evident that SN 2007pk experienced stronger interaction than all other objects discussed so far higher density and larger winds, then w greater than the other objects). Therefore, considering the estimates for SN 2007od (Inserra et al. 2011) and SN 2009bw (Inserra et al. 2012a), and finally comparing the inferred values, we roughly estimate a mass loss rate of $\dot{M} \gtrsim 10^{-5}$ $M_\odot$ yr^{-1} for SN 2007pk.

5.3. Is SN 2010aj without interaction?

The only object of the sample without signs of early interaction is SN 2010aj (although its first spectrum was obtained 3 weeks after the core-collapse). Distinctive features of SN 2010aj are a steep decline in the late light curve (although we believe the SN has not yet entered the nebular phase) and the redder V–I colours at late phases. For this object one could speculate that early dust formation occurred, like in the case of SN 2007od. Such an early dust formation episode suggests the presence of a CDS, implying previous ($\lesssim 80$d) interaction with a CSM produced through a

mass loss event occurred ~280 yr before the explosion (using the same wind properties and CSM velocity as for SN 2007od). Considering that the last spectrum does not show signature of SN nebular lines, and that dust formation during the nebular phase may be relatively common in luminous type II SNe (note that also in SN 1995ad there is an increase of the late time light curve decline rate, and that the presence of CO molecules has been reported, see Spyromilio & Leibundgut 1996) we consider this scenario not unreasonable.

5.4. Constraining the progenitor of luminous type II SNe from nebular spectra

In nebular spectra of CC-SNe the flux ratio R = [Ca II] $\lambda\lambda7291,7324$ / [O I] $\lambda\lambda6300,6364$ is a useful diagnostic for the mass of the core (Fransson & Chevalier 1989, 1987) and consequently for estimating the progenitor mass, with small ratios corresponding to higher main sequence masses as recently confirmed in the model of Jerkstrand et al. (2012). In SN 1987A a ratio $R \sim 3$ was found (Elmhamdi et al. 2003), for the faint SN 2005cs it was $R \sim 4.2\pm0.6$ (Pastorello et al. 2009), while for SNe 1992H and 1999em we computed values of $R \sim 1.6$ and $R \sim 4.7$, respectively. We computed this ratio only for those SNe where the lines were clearly detectable, then SN 1995ad has a ratio R of ~ 4.0 and SN 1996W of ~ 2.3, suggesting that the progenitor

mass is quite normal for the first object and slightly higher for the second one. This result is consistent with the higher amount of ^{56}Ni than the other objects, making SN 1996W similar to the bright type IIP SN 1992H (Clocchiatti et al. 1996). Following the similarities in ^{56}Ni mass and R between these two objects we can constrain the envelope mass of SN 1996W to be between 11 and 15M$_\odot$. The analyses reported in this paper suggest also that SN 2007pk could have a progenitor different from the other SNe. This object has in common with the sample only the high luminosity at peak but shows a different spectrophotometric evolution.

Taking the information reported above into account, we conclude that weak interaction episodes between ejecta and CSM at early epochs are relatively common in type II SNe.
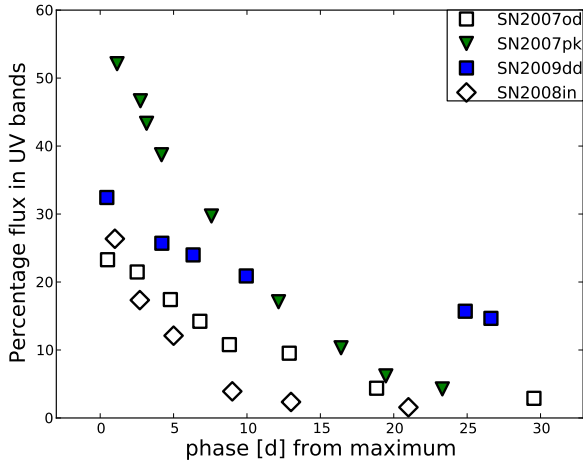

Fig. 22. Flux contribution of UV bands (uvw2, uvm2, uvw1) to the UV-to-I bolometric light curve for two out of five SNe of the sample and the normal type IIP SN 2008in.

5.5. Explosion and progenitor parameters

Using the well-tested approach applied to other CC-SNe (e.g. SNe 2005cs, 2007od, 2009bw, and 2009E; see Pastorello et al. 2009; Inserra et al. 2011, 2012a; Pastorello et al. 2012), we estimated the physical parameters of the SN and its progenitor (e.g. the ejected mass, the progenitor radius, and the explosion energy) for our sample of CC-SNe by performing a model/data comparison. This is based on a simultaneous χ^2 fit of the main CC-SN observables (namely, the bolometric light curve, the evolution of the photospheric velocity and the continuum temperature at the photosphere). We excluded SNe 2007pk and 1996W from the fitting procedure because the observational data are not sufficient or non suitable for the model/data comparison.

Two codes are employed to calculate the CC-SN models used for the comparison. The first one is the semi-analytic code described in Zampieri et al. (2003), which is used to perform preparatory studies to explore the parameter space describing the CC-SN progenitor at the explosion. The second one, used to compute a tighter grid of more accurate models is a new relativistic, radiation-hydrodynamics Lagrangian code, whose main features are (for details see Pumo et al. 2010; Pumo & Zampieri 2011): 1) an accurate treatment of radiative transfer coupled to relativistic hydrodynamics, 2) a self-consistent treatment of the evolution of ejected material taking into account the

gravitational effects of the central compact remnant, and 3) a fully implicit Lagrangian approach to the solution of the coupled non-linear finite difference system of relativistic radiation-hydro equations.

The modelling with these two codes is appropriate if the emission from the CC-SN is dominated by the expanding ejecta. For our sample, the contamination from interaction and/or formation of dust may in part affect the observables of our sample of CC-SNe, so it may not be possible to reproduce all the observed features perfectly. However, in our sample there is no evidence that these effects dominate during most of the photospheric phase. Hence, as already made for the two similar events SNe 2007od and 2009bw (cfr. Inserra et al. 2011, 2012a), we assume in the following that our modelling can be applied to our sample of CC-SNe, returning a reliable estimate of the main physical parameters of these events.

The values of the shock breakout epoch and distance modulus reported in Sect. 2 are used to fix the explosion epoch and to compute the bolometric luminosity of our sample of CC-SNe. For each SN of our sample, we obtained the best-fit models reported in Fig.s 24 25 & 26, and summarise the parameters in Table 7.

The agreement between our best-fit models and the observed light curve and photospheric temperature is quite satisfactory, except at early epochs ($\lesssim$ 20-40 d, cf. top and bottom panels of Fig.s 24, 25 & 26). The early time discrepancy may be linked to some ejecta-CSM interaction leading to a luminosity excess (for details see also Inserra et al. 2012a, and references therein), and to the approximate initial density profile used in our simulations, which does not reproduce correctly the radial profile of the outermost high-velocity shell of the ejecta formed after shock
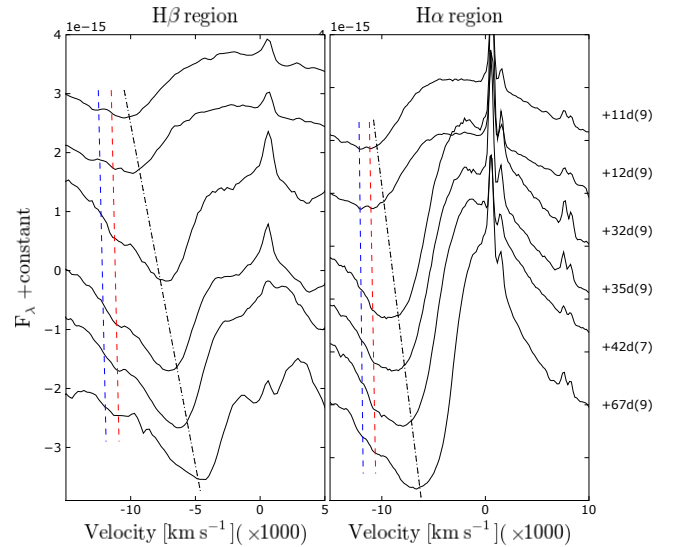

Fig. 23. Blow-up of the 4600Å (left-hand panel) and 6200Å (right-hand panel) spectral regions during the plateau phase of SN 1996W. The x-axes are in expansion velocity coordinates with respect to the rest-frame position of Hβ and Hα, respectively. To guide the eye, two dash-dotted lines are drawn in the spectra marking the position of minimum of the strongest absorption feature, while two red dashed lines, at comparable velocities, follow the HV Hα and Hβ features ($\sim$11500 km s^{-1}). The blue dashed lines is tied to the second HV feature at $\sim$12500 km s^{-1}, which is visible only in the Hα region.

breakout (cfr. Pumo & Zampieri 2011). For this last reason, in the χ^2 fit we did not include the line velocity measurements taken during the first 20-40 d.

Indeed, the discrepancies between the simulated photospheric velocity and the data could be explained in terms of an interaction creating a pseudo-photosphere at a larger radius, linked to the region of lines formation and non to the continuos. Hence at a higher velocity (by $\sim$ 3000, 2000, 1300 km s^{-1} for SNe 2009dd, 2010aj and 1995ad, respectively), than expected by the model (cf. blue-dotted line of middle panel of Fig.s 24, 25 & 26).

For SN 2010aj the low amount of ^{56}Ni and the probable presence of dust at relatively early phase (after $\sim$ 100 d) fit reasonably well with the mass loss and explosion expected for a SAGB star with an initial (ZAMS) mass close to the upper limit of this class of stars (see Pumo et al. 2009, for details).
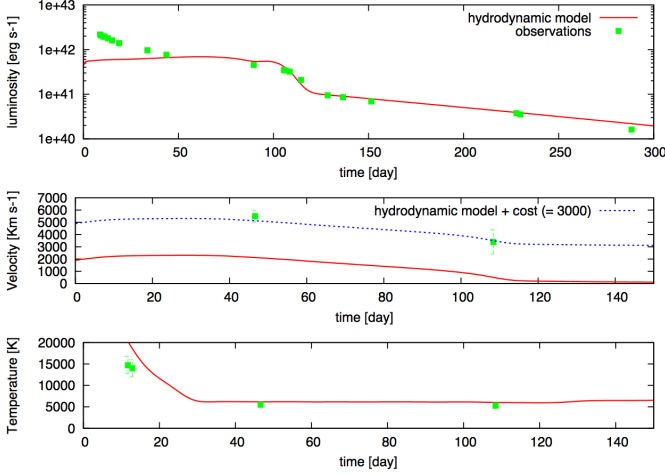

Fig. 24. Comparison of the evolution of the main observables of SN 2009dd with the best-fit models computed with the general-relativistic, radiation-hydrodynamics code (total energy $\sim$ 0.2 foe, initial radius 5×10^{13} cm, envelope mass 8 M$_\odot$). Top, middle, and bottom panels show the bolometric light curve, the photospheric velocity, and the photospheric temperature as a function of time. To estimate the photospheric velocity from observations, we used the value inferred from the Fe II lines (see text for further details).
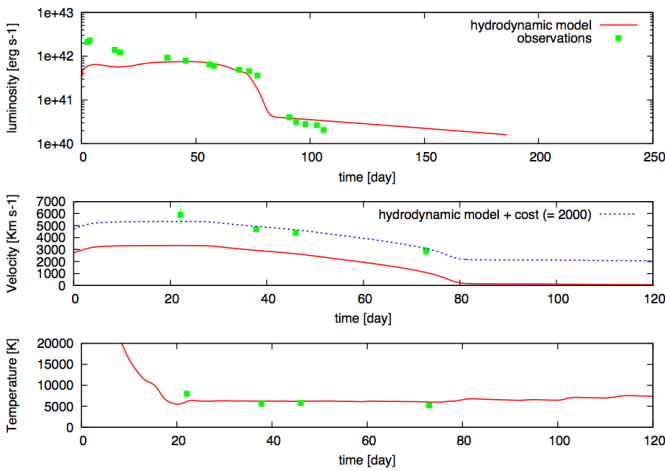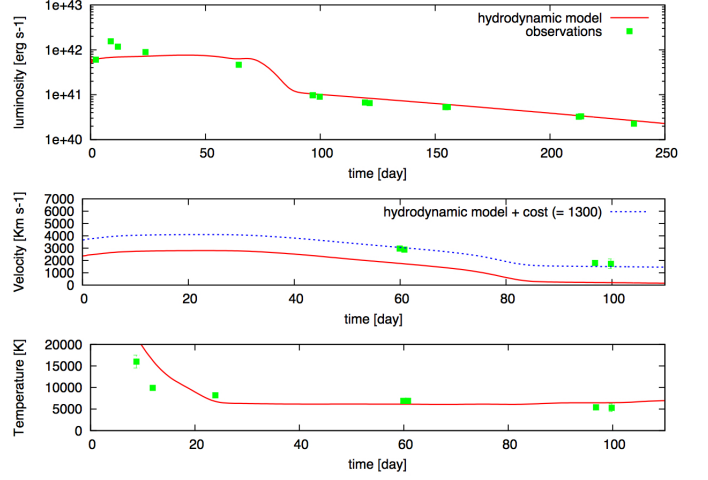

Fig. 26. As for Fig. 24, but for SN 1995ad. The best-fit model evaluated using the general-relativistic, radiation-hydrodynamics code has an initial radius of 5×10^{13} cm, a total energy $\sim$ 0.2 foe, and an envelope mass of 5 M$_\odot$.

For the other two SNe, the values of the modelling parameters reported above are consistent with both a SAGB progenitor and an iron CC-SN having a progenitor with an initial mass close to the lower limit for this class. Both scenarios are reliable, even if the first one poorly explains the amount of ^{56}Ni (e.g. Wanajo et al. 2009) and the second one may fail to explain the relatively low ejecta mass of SN 1995ad and the CO molecules observed during the nebular phase (Spyromilio & Leibundgut 1996). However, in both cases the progenitors have a radius at the explosion of $\sim 2 - 5 \times 10^{13}$ cm, which falls into the RSG class.

6. Conclusions

In this paper we have presented photometric and spectroscopic observations of three recent type II SNe (SNe 2009dd, 2007pk and 2010aj) together with previously unpublished data of SNe 1995ad and 1996W. Together with SNe 2007od and 2009bw, we have shown that they belong to a group of relatively bright type II SNe. The classification of these transients requires good timing because of the short period of visibility of the spectral features linked to the interaction. For this reason, we may consider the temporal coverage of our supernova sample not ideal. However, considering the full sample, we have homogenous properties, and provide a reasonably complete picture of the photometric and spectroscopic evolution of this small group of H-rich core-collapse SNe.

We have shown that they have luminous peak magnitudes (between M$_B$ = -18.70 and M$_B$ = -17.18), quite short duration of the plateau (between 30 and 100 days) and a wide range of ^{56}Ni masses (from 1.6×10^{-1} to 7×10^{-3} M$_\odot$). Three out of five objects follow the late time decay of the ^{56}Co supporting the interpretation that the tails are powered by radioactive ^{56}Co decay

Fig. 25. As for Fig. 24, but for SN 2010aj. The best-fit model evaluated using the general-relativistic, radiation-hydrodynamics code has an initial radius of 2×10^{13} cm, a total energy $\sim$ 0.5 foe, and an envelope mass of 9.5 M$_\odot$.

and making us confident that the ^{56}Ni estimates reported above are correct. Only SN 2010aj does not follow the same decline rate as the other objects. This is probably a sign of dust formation, although we do not have IR data to confirm this claim. Their spectra evolve like those of normal type II SNe in the detected transitions, the expansion velocities, and the blackbody temperature reached during the plateau phase (T$\sim$5000 ^{o}K). All SNe in the sample probably exploded in locations with grossly solar metallicity.

Direct or indirect clues of interaction have been clearly identified in the photospheric spectra of four out of five objects from the early phases ($\sim$11d) onwards. The HV features found are similar to those observed in SN 2004dj and SN 1999em (Chugai et al. 2007) and suggest early interaction with a low density CSM. For SN 2007pk we observed a spectral transition from a type IIn SN to a standard type II SN, making this object a rare example of the transition between these two core-collapse SN sub-types. In addition, SN 2009dd and SN 2007pk have significant UV flux, larger than that of SN 2007od (see Inserra et al. 2011) and SN 2007pk is also quite luminous at the X-ray wavelengths. Based on these clues, and the not very remarkable changes in the light curve (see Moriya et al. 2011) we roughly estimate the average mass loss rate during the pre-SN evolution to be in the range $10^{-6} \lesssim M_\odot \lesssim 10^{-5}$, consistent with the presumed (see below) SN progenitor.

Modelling of SNe 2009dd, 2010aj and 1995ad gives us ejecta masses in the range of 5.0–9.5 M$_\odot$ corresponding to an initial mass of the progenitors of the order of 7.0–12.5 M$_\odot$. These are marginally consistent with either SAGB stars or RSGs exploded as Fe CC-SN, explaining most properties (early interaction, ^{56}Ni mass and CNO elements) of these objects. Otherwise the progenitor of SN 2007pk and SN 1996W are different because of different observables: the spectral evolution and luminosity for the case of SN 2007pk; the high ^{56}Ni mass and the lower value $R\sim$ 2.3 in the case of SN 1996W. The unsatisfactory fit of the velocity during the entire photospheric phase strengthens the idea of ejecta–CSM interaction. In fact, the interaction could have caused the formation of a pseudo-photosphere at a radius larger than predicted by the model.

The SNe analysed here share only the high luminosity and the short plateau duration suggesting a sample which is far from being homogenous though still consistent with the bright branch of type II SNe. Our study has revealed: 1) direct or indirect evidences of early weak CSM interaction in 4 out of 5 objects; 2) a particular evolution of SN 2007pk highlighting the spectral transition from a type IIn to a standard type II; 3) quite high UV fluxes; 4) progenitors similar to those of most type II SNe. These sample suggests as luminous type II SNe could be the link between standard type IIP and strongly interacting type IIn events.

Acknowledgments

References

Jerkstrand, A., Fransson, C., Maguire, K., et al. 2012, A&A, 546, A28
Arnett, W. D., 1996, Supernovae and Nucleosynthesis, Princeton University Press, Princeton
Arnett, W. D., Bahcall, J. N., Kirshner, R. P., & Woosley, S. E. 1989, ARA&A, 27, 629
Asplund, M., Grevesse, N., Sauval, A. J., & Scott, P. 2009, ARA&A, 47, 481
Balinskaia, I. S., Bychkov, K. V., & Neizvestnyi, S. I. 1980, A&A, 85, L19
Barbon, R., Ciatti, F., & Rosino, L. 1979, A&A, 72, 287
Baron, E., Branch, D., Hauschildt, P. H., et al. 2000, ApJ, 545, 444
Botticella, M. T., Trundle, C., Pastorello, A., et al. 2010, ApJ, 717, L52
Broughton, J. 1998, IAU Circ., 6852, 2
Cappellaro, E., Danziger, I. J., & Turatto, M. 1995, MNRAS, 277, 106
Cappellaro, E., Mazzali, P. A., Benetti, S., et al. 1997, A&A, 328, 203
Cenko, S. B., Cobb, B. E., Kleiser, I. K., & Filippenko, A. V. 2010, Central Bureau Electronic Telegrams, 2209, 1
Chandra, P., & Soderberg, A. 2007, The Astronomer's Telegram, 1271, 1
Chevalier, R. A., & Fransson, C. 1994, ApJ, 420, 268
Chugai, N. N., Chevalier, R. A., & Utrobin, V. P. 2007, ApJ, 662, 1136
Chugai N. N., 1994, Circumstellar Media in Late Stages of Stellar Evolution, 148.
Clocchiatti, A., Benetti, S., Wheeler, J. C., et al. 1996, SN 2010aj, 111, 1286
Cortini, G. and Dimai, A. 2009, CBET 1764, 1
Elias-Rosa, N., van Dyk, S.D., Agnoletto, I., and Benetti, S. 2009, CBET 1765, 1
Elmhamdi, A., Danziger, I. J., Chugai, N., et al. 2003, MNRAS, 338, 939
Evans, R., Benetti, S., & Grupe, D. 1995, IAU Circ., 6239, 1
Fassia, A., Meikle, W. P. S., Chugai, N., et al. 2001, MNRAS, 325, 907
Fransson, C., & Chevalier, R. A. 1989, ApJ, 343, 323
Fransson, C., & Chevalier, R. A. 1987, ApJ, 322, L15
Gal-Yam, A., & Leonard, D. C. 2009, Nature, 458, 865
Gal-Yam, A., Leonard, D. C., Fox, D. B., et al. 2007, ApJ, 656, 372
Hakobyan, A. A., Mamon, G. A., Petrosian, A. R., Kunth, D., Turatto, M. 2009, A&A, 508, 1259
Hamuy, M. 2003, ApJ, 582, 905
Harutyunyan, A. H., Pfahler, P., Pastorello, A., et al. 2008, A&A, 488, 383
Heger, A., Fryer, C. L., Woosley, S. E., Langer, N., & Hartmann, D. H. 2003, ApJ, 591, 288
Immler, S., Russell, B.R., and Brown, P.J. 2009, The Astronomer's Telegram 2106, 1
Immler, S., Pooley, D., Brown, P. J., Li, W., & Filippenko, A. V. 2007, The Astronomer's Telegram, 1284, 1
Inserra, C., Turatto, M., Pastorello, A., et al. 2012, MNRAS, 422, 1122
Inserra, C., Baron, E., & Turatto, M. 2012, MNRAS, 422, 1178
Inserra, C., Turatto, M., Pastorello, A., et al. 2011, MNRAS, 417, 261
Landolt A. U., 1992, AJ, 104, 340
Li, W., Leaman, J., Chornock, R., et al. 2011, MNRAS, 412, 1441
Li, W., Jha, S., Filippenko, A. V., et al. 2006, PASP, 118, 37
Li, W. D., Qiu, Y. L., Qiao, Q. Y., et al. 1996, IAU Circ., 6379, 1
López-Sánchez, Á. R., & Esteban, C. 2010, A&A, 517, A85
Maguire, K., di Carlo, E., Smartt, S. J., et al. 2010, MNRAS, 404, 981
McNaught, R. H., & Pollas, C. 1995, IAU Circ., 6242, 2
Milisavljevic, D., Fesen, R. A., Kirshner, R. P., Challis, P.2009, ApJ, 692, 839
Milisavljevic, D., Fesen, R., Chevalier, R., Kirshner, R., Challis, P., Turatto, M, 2012, ApJ, in press (arXiv:1203.0006)

Moriya, T., Tominaga, N., Blinnikov, S. I., Baklanov, P. V., & Sorokina, E. I. 2011, MNRAS, 415, 199

Mould, J. R., Huchra, J. P., Freedman, W. L., et al. 2000, ApJ, 529, 786

Newton, J., Puckett, T., & Orff, T. 2010, Central Bureau Electronic Telegrams, 2201, 1

Parisky, X., Li, W., Filippenko, A. V., Silverman, J. M., Foley, R. J. 2007, Central Bureau Electronic Telegrams, 1129,

Pastorello, A., Pumo, M. L., Navasardyan, H., et al. 2012, A&A, 537, A141

Pastorello, A., Valenti, S., Zampieri, L., et al. 2009, MNRAS, 394, 2266

Pastorello, A., Zampieri, L., Turatto, M., et al. 2004, MNRAS, 347, 74

Patat, F., Barbon, R., Cappellaro, E., & Turatto, M. 1994, A&A, 282, 731

Pettini, M., & Pagel, B. E. J. 2004, MNRAS, 348, L59

Pignata, G., Patat, F., Benetti, S., et al. 2004, MNRAS, 355, 178

Poole, T. S., Breeveld, A. A., Page, M. J., et al. 2008, MNRAS, 383, 627

Poznanski, D., Ganeshalingam, M., Silverman, J. M., & Filippenko, A. V. 2011, MNRAS, 415, L81

Pritchard, T. A., Roming, P. W. A., Brown, P. J., et al. 2012, ApJ, 750, 128

Pumo, M. L., & Zampieri, L. 2011, ApJ, 741, 41

Pumo, M. L., Zampieri, L., & Turatto, M. 2010, Mem. Soc. Astron. Italiana Supplementi, 14, 123

Pumo, M. L., Turatto, M., Botticella, M. T., et al. 2009, ApJ, 705, L138

Pumo, M. L. 2007, Mem. Soc. Astron. Italiana, 78, 689

Pumo, M. L. 2006, Ph.D. Thesis, Univ. Catania

Richardson, D., Branch, D., Casebeer, D., et al. 2002, SN 2010aj, 123, 745

Roy, R., Kumar, B., Benetti, S., et al. 2011, ApJ, 736, 76

Schlegel, D. J., Finkbeiner, D. P., & Davis, M. 1998, ApJ, 500, 525

Schlegel, E. M. 1990, MNRAS, 244, 269

Smartt, S. J. 2009, ARA&A, 47, 63

Spyromilio, J., & Leibundgut, B. 1996, MNRAS, 283, L89

Stockdale, C. J., Weiler, K. W., Immler, S., et al. 2009, The Astronomer's Telegram, 2016, 1

Stritzinger, M., Hamuy, M., Suntzeff, N. B., et al. 2002, SN 2010aj, 124, 2100

Suntzeff, N. B., Ruiz, M.-T., & Depoy, D. 1996, IAU Circ., 6380, 2

Turatto, M., Benetti, S., Cappellaro, E., 2003, in Hillebrandt W., Leibundgut B., eds. ESO Astrophys. Symp. Vol. XVII, From Twilight to Highlight: the Physics of Supernovae. Springer-Verlag, Berlin, p. 200

Wanajo, S., Nomoto, K., Janka, H.-T., Kitaura, F. S., Mülller, B. 2009, ApJ, 695, 208

Woosley, S. E., Heger, A., & Weaver, T. A. 2002, Reviews of Modern Physics, 74, 1015

Woosley, S. E., Hartmann, D., & Pinto, P. A. 1989, ApJ, 346, 395

Woosley, S. E., & Weaver, T. A. 1986, ARA&A, 24, 205

Zampieri, L., Mucciarelli, P., Pastorello, A., et al. 2005, MNRAS, 364, 1419

Zampieri, L., Pastorello, A., Turatto, M., et al. 2003, MNRAS, 338, 711

Appendix A: Online material

Table A.1. Magnitudes of the local sequence stars in the field of SN 2009dd (cfr. Fig. 1). The errors in brackets are the r.m.s.

ID	U	B	V	R	I
1	16.24 (.07)	17.01 (.02)	16.34 (.01)	16.11 (.01)	15.76 (.02)
2	15.64 (.05)	15.23 (.01)	14.26 (.02)	13.63 (.01)	13.19 (.01)
3	-	19.07 (.02)	17.72 (.02)	16.89 (.01)	16.28 (.02)
4	16.97 (.01)	16.41 (.02)	15.48 (.02)	15.04 (.01)	14.59 (.01)
5	-	19.75 (.02)	19.09 (.02)	18.68 (.02)	18.48 (.03)
6	-	19.91 (.03)	19.06 (.02)	18.32 (.02)	17.77 (.02)
7	-	21.07 (.03)	19.60 (.02)	18.39 (.01)	16.84 (.02)
8	-	20.47 (.02)	19.57 (.02)	18.99 (.02)	18.40 (.02)
9	18.58(-)	17.66 (.02)	16.25 (.03)	15.61 (.01)	14.96 (.02)
10	19.80 (-)	19.00 (.02)	17.95 (.03)	17.52 (.01)	17.12 (.02)

Table A.2. Magnitudes of the local sequence stars in the field of SN 2007pk (cfr. Fig. 2).

ID	U	B	V	R	I
1	17.00 (.02)	17.11 (.02)	16.53 (.02)	16.21 (.02)	15.82 (.02)
2	19.12 (.02)	18.61 (.03)	17.71 (.01)	17.08 (.03)	16.70 (.02)
3	17.26 (.03)	17.08 (.02)	16.34 (.02)	15.80 (.03)	15.52 (.02)
4	14.70 (.02)	14.79 (.02)	14.35 (.03)	13.85 (.01)	13.54 (.02)
5	16.16 (.02)	16.20 (.02)	15.56 (.02)	15.22 (.03)	14.77 (.03)
6	18.22 (.02)	17.89 (.03)	16.95 (.02)	16.56 (.03)	16.13 (.02)
7	15.81 (.03)	15.86 (.03)	15.26 (.01)	14.93 (.02)	14.69 (.01)
8	15.05 (.02)	14.40 (.03)	13.42 (.03)	12.84 (.02)	12.38 (.01)
9	17.14 (.02)	16.92 (.02)	16.41 (.02)	16.13 (.02)	15.86 (.01)
10	17.54 (.02)	17.48 (.04)	16.79 (.01)	16.45 (.02)	16.14 (.02)
11	17.40 (.02)	17.40 (.03)	16.68 (.01)	16.37 (.02)	16.18 (.05)
12	20.50 (.03)	19.42 (.03)	18.20 (.02)	17.47 (.03)	16.82 (.02)
13	19.20 (.03)	18.76 (.02)	17.90 (.01)	17.42 (.02)	16.90 (.03)

Table A.3. As Tab. A.1 but for SN 2010aj (cfr. Fig. 3).

ID	U	B	V	R	I
1	19.14 (.06)	18.52 (.03)	17.62 (.01)	16.99 (.01)	16.48 (.01)
2	17.72 (.06)	17.68 (.02)	17.09 (.04)	16.80 (.01)	16.42 (.02)
3	19.00 (-)	17.91 (.05)	16.39 (.02)	16.31 (.01)	16.07 (.02)
4	18.72 (-)	17.74 (.04)	16.58 (.04)	15.94 (.01)	15.37 (.01)
5	16.90 (.01)	16.77 (.01)	16.05 (.02)	15.62 (.02)	15.24 (.01)
6	14.97 (-)	15.03 (.02)	14.48 (.01)	14.17 (.01)	13.81 (.01)
7	18.89 (-)	18.72 (.01)	17.69 (.07)	17.26 (.01)	16.66 (.07)
8	18.95 (-)	19.27 (.02)	18.66 (.02)	18.37 (.01)	17.83 (.08)
9	18.87 (-)	18.06 (.02)	17.35 (.05)	16.76 (.01)	16.64 (.01)
10	17.91 (-)	18.44 (.04)	17.92 (.01)	17.63 (.01)	17.01 (.08)

Table A.4. Magnitudes of the local sequence stars in the field of SN 1995ad (cfr. Fig. 4).

ID	B	V	R	I
1	17.92 (.02)	17.31 (.01)	16.96 (.01)	16.65 (.01)
2	17.98 (.01)	17.61 (.01)	17.28 (.01)	16.89 (.01)
3	16.25 (.01)	15.29 (.01)	14.78 (.01)	14.29 (.01)
4	15.88 (.01)	15.39 (.01)	15.11 (.01)	14.78 (.01)
5	17.93 (.02)	17.33 (.01)	16.97 (.01)	16.62 (.04)
6	18.63 (.02)	18.08 (.01)	17.74 (.01)	17.43 (.01)
7	19.21 (.06)	17.72 (.08)	16.56 (.07)	15.17 (.06)
8	18.80 (.02)	18.30 (.07)	18.01 (.05)	17.73 (.02)
9	19.59 (.04)	18.14 (.08)	17.23 (.05)	16.32 (.04)
11	17.78 (.03)	17.16 (.05)	16.80 (.03)	16.40 (.07)
12	16.74 (.01)	16.18 (.05)	15.86 (.06)	15.47 (.10)

Table A.5. Magnitudes of the local sequence stars in the field of SN 1996W (cfr. Fig. 5).

ID	U	B	V	R	I
2	19.18 (.02)	18.28 (.01)	17.29 (.01)	16.71 (.01)	16.22 (.01)
3	16.90 (.04)	15.94 (.01)	14.90 (.01)	14.28 (.01)	13.76 (.01)
4	19.08 (.02)	18.94 (.02)	18.14 (.01)	17.76 (.01)	17.39 (.02)
5	19.22 (.02)	19.36 (.03)	18.77 (.02)	18.40 (.01)	18.04 (.02)
6	20.03 (.03)	19.88 (.04)	19.29 (.03)	18.83 (.01)	18.47 (.02)

Table A.6. Journal of spectroscopic observations of the SNe in our sample.

Date	JD +2400000	Phase[*] (days)	Instrumental [◦] configuration	Range (Å)	Resolution[†] (Å)
			SN 2009dd		
09/04/14	54936.7	11.2	NOT+ALFOSC+gm4	3480-7500	13
09/04/16	54938.4	12.9	CAHA+CAFOS+b200	3400-8700	11.3
09/05/20	54971.6	46.1	TNG+DOLORES+LRB,LRR	3700-9220	15
09/07/20	55033.4	107.9	TNG+DOLORES+LRB,LRR	3800-10100	15
09/11/19	55155.7	230.2	CAHA+CAFOS+g200	4000-9700	9.5
09/11/21	55157.7	232.2	TNG+DOLORES+LRR	5100-9300	10.3
10/05/18	55334.5	409.0	TNG+DOLORES+LRR	5030-9270	9.8
			SN 2007pk		
07/11/11	54416.3	4.3	Copernico + AFOSC+gm4	3650-7800	24
07/11/12	54417.5	5.5	Copernico + AFOSC+gm2	5320-9080	36
07/11/16	54421.4	8.4	TNG+DOLORES+LRB,LRR[‡]	3400-9000	14
07/12/05	54439.5	27.5	Copernico +AFOSC+gm4,gm2	3700-9050	25
07/12/28	54463.3	51.3	Copernico +AFOSC+gm4,gm2	3780-9180	23
08/01/11	54477.4	65.4	NOT+ALFOSC+gm4	3580-9120	14
08/01/12	54478.4	66.4	TNG+NICS+ij	8660-13480	18
08/01/28	54494.3	82.3	Copernico +AFOSC+gm4	3670-7770	23
08/09/05	54714.5	302.5	TNG+DOLORES+LRR	5150-10230	16
08/10/02	54741.7	329.7	Palomar+DBSP+red	5800-9990	17
			SN 2010aj		
10/03/30	55287.6	22.1	WHT+ISIS+R300B,R158R	3130-11130	5.4-6.3
10/04/14	55303.3	37.8	NTT+EFOSC2+gm16	3800-7500	13
10/04/24	55311.5	46.0	TNG+DOLORES+LRB,LRR	3380-9900	10
10/05/21	55338.5	73.0	TNG+DOLORES+LRB,LRR	3500-9700	10
11/02/11	55604.3	356.8	NTT+EFOSC2+gm13	3650-9300	17
			SN 1995ad		
95/09/29	49989.8	8.8	ESO 1.5+B&C+gr2	3930-7790	5
95/10/02	49992.9	11.9	ESO 3.6+EFOSC1+B300,R300	3750-9920	14+17
95/10/14	50004.9	23.9	ESO 3.6+EFOSC1+B300	3750-6940	19
95/11/19	50040.8	59.9	ESO 1.5+B&C+gr2	3100-10710	10
95/11/20	50041.8	60.8	ESO 1.5+B&C+gr2	3100-10710	14
95/12/26	50077.8	96.8	MPG-ESO 2.2+EFOSC2+gr3,gr5,gr1	3720-9040	11+11+60
95/12/29	50080.8	99.8	ESO 3.6+EFOSC1+B300,R300	3740-9910	14+17
96/01/21	50103.7	122.7	ESO 1.5+B&C+gr2	3460-11100	9
96/02/18	50131.7	150.7	MPG-ESO 2.2+EFOSC2+gr5,gr6	3350-8980	11+11
96/02/19	50132.7	151.7	ESO 1.5+B&C+gr2	3040-10000	9
96/02/20	50133.7	152.7	ESO 1.5+B&C+gr2	3040-10000	9
97/02/11	50490.6	509.6	ESO 3.6+EFOSC1+R300	6000-9850	23
			SN 1996W		
96/04/18	50191.6	11.6	ESO 1.5+B&C+gr2	3160-10650	9
96/04/19	50192.6	12.6	ESO 1.5+B&C+gr2	3160-10650	9
96/06/21	50195.4	15.4	Copernico+B&C+150tr.	4250-8600	29
96/04/24	50198.4	18.1	ESO 1.5+B&C+gr2	3130-10430	9
96/04/25	50198.6	18.5	ESO 1.5+B&C+gr2	3130-10430	9
96/05/09	50212.5	32.5	ESO 1.5+B&C+gr2	3120-10590	9
96/05/12	50215.6	35.6	ESO 1.5+B&C+gr2	3120-10590	9
96/05/19	50222.6	42.6	MPG-ESO 2.2+EFOSC2+gr5,gr6	2850-9050	7+7
96/06/12	50247.5	67.5	ESO 1.5+B&C+gr2	2900-10460	9
96/12/15	50432.8	252.8	MPG-ESO 2.2+EFOSC2+gr6	3840-7980	10
97/01/30	50478.5	298.5	Danish 1.54+DFOSC+gr5	5000-10180	8
97/02/13	50492.7	312.7	MPG-ESO 2.2+EFOSC2+gr5	5220-9280	9

[*] with respect to the explosion epochs (cfr. Tab. 7)
[◦] coded as in Tab. 1
[†] measured from the full-width at half maximum (FWHM) of the night sky lines